

# Hybrid Downlink Beamforming with Outage Constraints under Imperfect CSI using Model-Driven Deep Learning

Lukas Schynol<sup>1</sup> (*Graduate Student Member, IEEE*) and Marius Pesavento<sup>1</sup> (*Senior Member, IEEE*)

<sup>1</sup>Technical University of Darmstadt, Darmstadt, Germany

CORRESPONDING AUTHOR: Lukas Schynol (e-mail: lschynol@nt.tu-darmstadt.de).

This work was financially supported by the Federal Ministry of Research, Technology and Space of Germany in the project "Open6GHub+" (grant no. 16KIS2407).

**ABSTRACT** We consider energy-efficient multi-user hybrid downlink beamforming (BF) and power allocation under imperfect channel state information (CSI) and probabilistic outage constraints. In this domain, classical optimization methods resort to computationally costly conic optimization problems. Meanwhile, generic deep network (DN) architectures lack interpretability and require large training data sets to generalize well. In this paper, we therefore propose a lightweight model-aided deep learning architecture based on a greedy selection algorithm for analog beam codewords. The architecture relies on an instance-adaptive augmentation of the signal model to estimate the impact of the CSI error. To learn the DN parameters, we derive a novel and efficient implicit representation of the nested constrained BF problem and prove sufficient conditions for the existence of the corresponding gradient. In the loss function, we utilize an annealing-based approximation of the outage compared to conventional quantile-based loss terms. This approximation adaptively anneals towards the exact probabilistic constraint depending on the current level of quality of service (QoS) violation. Simulations validate that the proposed DN can achieve the nominal outage level under CSI error due to channel estimation and channel compression, while allocating less power than benchmarks. Thereby, a single trained model generalizes to different numbers of users, QoS requirements and levels of CSI quality. We further show that the adaptive annealing-based loss function can accelerate the training and yield a better power-outage trade-off.

**INDEX TERMS** Deep unrolling with constraints, hybrid beamforming, multi-user MISO, probabilistic outage constraint, mixed-integer, implicit function differentiation

## I. Introduction

Downlink beamforming (BF) serves as a fundamental technology in modern wireless networks, including 3GPP 5G [1] and the upcoming 6G standard [2]. Nonetheless, large-scale multi-antenna systems, network densification and surging traffic demands led to an increased energy usage and cost [3], [4]. As such, energy efficiency is of marked interest in future wireless systems [5].

Considering these challenges, hybrid radio frequency (RF) front-ends that integrate low-dimensional digital processing with high-dimensional analog processing offer a compelling advantage. Hybrid BF architectures improve energy consumption and cost while achieving a spatial separation and throughput comparable to fully digital architectures [6], [7]. However, restrictions on the configuration of analog compo-

ments make it challenging to optimize beam patterns w.r.t. network utilities such as sum-rate or allocated power under quality of service (QoS) requirements in multi-user (MU) systems [8]. The problem is intensified in practical systems with a large number of antennas, e.g., systems operating millimeter wave or the upcoming 6G FR3 bands, where channel state information (CSI) degradation arises from factors such as estimation errors, quantization of feedback, time-varying fading or space and frequency subsampling of the channel [8], [9]. Classical approaches commonly tackle the resulting robust downlink BF problem by regularization and diagonal loading [10]–[12]. However, these approaches are not easily applicable in multi-user downlink scenarios with QoS constraints. Alternatively, robust methods based on conic optimization, which require knowledge of the error

distribution and are often computationally costly, have been explored, e.g., [9], [13]–[17].

In recent years, deep learning (DL) has thus been considered to address BF and power allocation in a computationally efficient manner [18]. To mitigate concerns regarding the black-box nature of generic deep network (DN) architectures and their generalization capability [19], recent work turns to the concept of model-aided DL and deep unrolling [20], [21]. By integrating existing domain knowledge and modifying classical algorithms with learnable components, model-aided DN architectures offer advantages in training data efficiency, generalization capability and explainability [22]. This motivates us to tackle energy-efficient and robust hybrid BF from the perspective of model-aided DL.

### A. Related Work

Hybrid BF is extensively discussed in the literature [6]. The majority of existing non-DL approaches decouple RF and baseband beamformers and either aim to maximize the sum-rate under power constraints, e.g., [7], [23], minimize the MMSE or reconstruct a desired beam pattern, e.g., [24], [25], see also [26].

Energy-efficient hybrid BF realized by power minimization under QoS constraints is investigated in [27]–[33]. In [27]–[29] and [30, Alg. 2], the MU multiple-input single-output (MISO) and MU multiple-input multiple-output (MIMO) problem is tackled by zero-forcing precoding and block diagonalization. Under certain conditions, block diagonalization and zero-forcing fully eliminate interference between user signals with digital precoding, thereby simplifying the problem substantially. However, when CSI uncertainty is present, full cancellation cannot be guaranteed, resulting in a degraded QoS level. Instead of block diagonalization, the algorithms in [30]–[32] and [33, Alg. 1] address QoS-constrained power minimization with a block-iterative approach, where the nested subproblems rely on conic and semidefinite programming. In [34], [35], the analog beams are restricted to a discrete set of codewords, enabling a particularly cost-efficient implementation. Algorithm 2 of [35] employs a greedy correction strategy for codeword selection, whereas [34] relaxes the codeword selection problem into a cone program with sparse regularization. Generally speaking, the corresponding optimization problems of all aforementioned methods assume perfect CSI.

To the best of our knowledge, the only non-DL-based work addressing robust *and* energy-efficient hybrid BF is [36], which investigates MU MIMO BF using a worst-case framework in two variants. The first applies a cutting-set method that iteratively solves conic optimization problems to construct a set of worst-case channels. The second reduces the complexity by leveraging block diagonalization, leading to a more conservative allocation of resources.

Considering these trade-offs, model-aided DL methods present an opportunity for robust BF. Most literature on fully digital or hybrid BF using DL focuses on sum-rate

maximization under power constraints, since power constraints are straightforward to implement by a projection. In the aforementioned, robustness is introduced by training with imperfect CSI data, e.g., [37], [38], by sample averaging [39], or by addressing uncertainty via the usage of statistical CSI [40], [41]. A projection approach, however, is not suitable for most QoS constraints due to their nonconvexity or probabilistic formulation. In [42], a model-aided DL framework leveraging uplink-downlink duality for QoS-constrained fully-digital BF is proposed. The authors design a DN that predicts the power allocation, which enables the recovery of precoders by the analytic solution structure, but only perfect CSI is considered. In [43], [44], sum-rate maximization in robust hybrid BF without QoS constraints is tackled by a worst-case max-min approach using unrolled projected gradient descent (PGD). The authors of [45] extend the work in [43], [44] for fully digital BF in an integrated sensing and communication system with QoS constraints. Thereby, a probabilistic outage constraint is converted into a worst-case error constraint and integrated into the unrolled DN architecture via the Lagrangian formulation. However, the accuracy of constraint satisfaction during testing remains uncertain. In [46], worst-case robust energy-efficient BF and antenna selection with a branch-and-bound algorithm and semidefinite programming is accelerated by branch selection using a graph neural network (GNN).

DL for BF that incorporate probabilistic outage constraints into the training objective are considered in [47]–[50]. In [47]–[49], generic DN architectures learn robust BF policies by embedding the outage constraint into the training objective as a penalty. Specifically, [47] and [48] employ a quantile-based formulation of the constraints for fully digital MU-MISO downlink BF, while [49] applies a fixed approximation of the outage probability for power allocation in multiple access. In contrast, [50] combines the quantile-based approach with primal-dual stochastic gradient descent/ascent for robust fully-digital BF, thereby avoiding the need to predefine penalty weights. In [51], a model-aided DN is trained to maximize a nominal quantile of the sum-rate, after which the maximum transmit power is bisected until the target QoS is achieved. The method does not support instance-dependent QoS constraints and the inclusion of differing QoS levels is not straightforward. We further observe that the approaches in [47]–[51] are only verified on systems with small arrays or low signal-to-interference-plus-noise ratio (SINR) requirements ( $\leq 0$  dB).

### B. Contributions

Motivated by the drawbacks of [47]–[51], we study energy-efficient MU hybrid downlink BF under probabilistic QoS constraints with model-aided DL, which, to our knowledge, has not been previously investigated. As in [34], [35], [52], but in contrast to the classical method for hybrid BF with QoS constraints under imperfect CSI in [36], the columns of

the analog beamformer are restricted to a discrete codebook (CB). Our contributions can be summarized as follows:

- Leveraging model-aided DL, we propose a novel DN architecture based on uplink-downlink duality for power minimization and precoding in hybrid BF under outage probability constraints. In contrast to the framework in [42] and similar succeeding works, we do not predict the power allocation and instead rely on an adaptive lightweight mapping of CSI using GNNs, thereby avoiding the second-order cone programming or semidefinite programming of classical approaches. Compared to previous works on QoS-constrained BF under imperfect CSI [45]–[51], the resultant models can adapt to various channels conditions with changing CSI quality, required SINR levels, the number of users, and supports instantaneous and statistical CSI. Crucially, our method does not rely on knowledge of the analytical CSI error distribution as in [45], [46].
- In the process, we derive a novel and efficient implicit representation for the underlying uplink BF and power minimization problem under QoS constraints and the corresponding gradient w.r.t. the CSI. We further prove sufficient conditions for the existence of the gradient.
- We propose an annealing-based approach that, unlike the fixed approximation used in [49], employs an adaptive annealing coefficient to integrate probabilistic constraints into DN training. The effectiveness of this method is demonstrated in comparison to conventional quantile-based implementations as in [47], [48], [50].
- We provide an extensive empirical comparison of the power-outage trade-off of our proposed method against benchmark algorithms. We further verify the generalization and adaptation capabilities of our proposed method under varying CSI quality, QoS requirements and number of users in the network.

Compared to our preliminary work in [53] that examines purely codebook-based BF, this work considers hybrid BF instead, thereby providing a novel representation of the underlying uplink BF problem to enable an efficient gradient computation during DN learning. In addition, we extensively validate our method with 5-fold cross validation, thereby proposing a convergence metric for the constrained training problem to ensure fairness and consistency between runs. We further provide empirical comparisons between the annealing-based and quantile-based probabilistic constraint implementation.

### C. Paper Structure

The remainder of the paper is structured as follows. In Sec. II, we specify the system model and define the investigated optimization problem. Building on the greedy hybrid BF approach [35] reviewed in Sec. III, we present the proposed architecture and its gradient based on a novel implicit representation in Sec. IV. In particular, we discuss

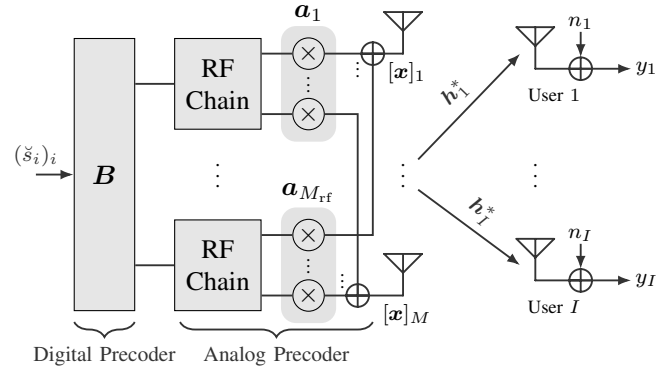


FIGURE 1. Diagram of the considered hybrid system model.

training with the proposed annealing-based loss function and provide a technical comparison to the prevailing approach for chance-constrained QoS constraints. Sec. V discusses empirical results and Sec. VI concludes this paper.

### D. Notation

Scalars, vectors and matrices are denoted as  $x$ ,  $\mathbf{x}$  and  $\mathbf{X}$ .  $[x]_i$  and  $[\mathbf{x}]_{i,j}$  represent the  $i$ th and  $(i, j)$ th element, respectively. The notation of functions follows the elements of their co-domain.  $[\mathbf{X}]_{i,:}$  and  $[\mathbf{X}]_{:,j}$  are the vectors resulting from slicing the  $i$ th row or  $j$ th column, while  $[\mathbf{x}]_{-i}$ ,  $[\mathbf{X}]_{-i,:}$  or  $[\mathbf{X}]_{:, -j}$  are the vector or matrix with the  $i$ th element, row or column excluded. Hadamard and Kronecker products are denoted by  $\odot$  and  $\otimes$ . We define  $\mathbb{P}(\cdot)$ ,  $\widehat{\mathbb{P}}(\cdot)$ ,  $\mathbb{E}(\cdot)$  and  $\widehat{\mathbb{E}}(\cdot)$  as probability, empirical probability, expected value and sample mean, respectively. The Jacobi matrix of a vector-valued function  $\mathbf{f}(\mathbf{x})$  is denoted as  $\mathbf{D}_{\mathbf{x}} \mathbf{f}(\mathbf{x})$ . Finally, an underline  $\underline{x}$  indicates the real-valued version of a complex variable  $x$ .

## II. System Model and Problem Formulation

### A. System Model

We consider a multi-user multiple-input single-output (MU MISO) downlink channel with an  $M$ -antenna hybrid digital-analog transmitter, which is equipped with  $M_{\text{rf}} \leq M$  RF chains, serving  $I$  single-antenna receivers as shown in Fig. 1. The transmitter allocates a transmit power  $p_i \geq 0$  to send symbol  $\check{s}_i \in \mathbb{C}$  to each user  $i$ , where  $\mathbb{E}(|\check{s}_i|^2) = 1$  and  $\mathbb{E}(\check{s}_i \check{s}_j^*) = 0$  for  $i \neq j$ , over a frequency-flat and block-fading channel  $\mathbf{h}_i^* \in \mathbb{C}^M$ .

For each user  $i$ , the transmitted signal is formed using a hybrid beamformer  $\mathbf{A}\mathbf{b}_i$ , where the matrix  $\mathbf{A} = [\mathbf{a}_1 \cdots \mathbf{a}_{M_{\text{rf}}}]$  is common to all users and consists of  $M_{\text{rf}}$  analog beamformers  $\mathbf{a}_r \in \mathcal{A}_{\text{rf}}$  selected from a discrete finite codebook  $\mathcal{A}_{\text{rf}} = \{\check{\mathbf{a}}_1, \dots, \check{\mathbf{a}}_A\}$ . The vector  $\mathbf{b}_i \in \mathbb{C}^{M_{\text{rf}}}$  is the digital precoder for user  $i$  and satisfies  $\|\mathbf{b}_i\|_2 = 1$  for  $i = 1, \dots, I$ . Given the total transmit signal  $\mathbf{x} = \sum_{i=1}^I \sqrt{p_i} \mathbf{A}\mathbf{b}_i \check{s}_i$ , the received signal  $y_i$  at user  $i$  including multi-user interference is [35]

$$y_i = \sqrt{p_i} \mathbf{h}_i^H \mathbf{A} \mathbf{b}_i \check{s}_i + \sum_{j \neq i} \sqrt{p_j} \mathbf{h}_i^H \mathbf{A} \mathbf{b}_j \check{s}_j + n_i. \quad (1)$$

Without loss of generality,  $n_i$  is modeled as additive white Gaussian noise with unit variance  $\mathbb{E}(|n_i|^2) = 1$ . Defining  $\mathbf{p} = [p_1 \cdots p_I]^T$  and  $\mathbf{B} = [\mathbf{b}_1 \cdots \mathbf{b}_I]^T$  for convenience, the resulting downlink SINR at user  $i$  is characterized by

$$\text{SINR}_i^{\text{DI}}(\mathbf{p}, \mathbf{B}, \mathbf{A}) = \frac{p_i \mathbf{b}_i^H \Psi_i(\mathbf{A}) \mathbf{b}_i}{\sum_{j \neq i} p_j \mathbf{b}_j^H \Psi_i(\mathbf{A}) \mathbf{b}_j + 1}. \quad (2)$$

Here, we define for  $i = 1, \dots, I$

$$\Psi_i(\mathbf{A}) = \mathbf{A}^H \mathbf{R}_i \mathbf{A}, \quad (3)$$

where  $\mathbf{R}_i \succeq \mathbf{0}$ . In case instantaneous SINR is considered,  $\mathbf{R}_i = \mathbf{h}_i \mathbf{h}_i^H$  is the outer channel product. Alternatively, in case statistical CSI is available,  $\mathbf{R}_i$  can be substituted by the channel covariance  $\mathbf{R}_i = \mathbb{E}(\mathbf{h}_i \mathbf{h}_i^H)$  such that  $\Psi_i(\mathbf{A})$  is the channel covariance *seen* by the digital precoder, leading to  $\text{SINR}_i^{\text{DI}}(\mathbf{p}, \mathbf{B}, \mathbf{A})$  being an approximation of the average SINR [54].

### B. Energy-efficient Hybrid Beamforming with Exact CSI

First, the case of availability of exact CSI at the transmitter is considered. The goal is to find the power allocation  $\mathbf{p}^*$  and corresponding beamformers  $(\mathbf{A}^*, \mathbf{B}^*)$  such that the weighted sum-power  $\mathbf{p}^T \mathbf{w}(\mathbf{A}, \mathbf{B})$  is minimized while a minimum SINR  $\gamma_i > 0$  at each user  $i$  is guaranteed. The weights  $\mathbf{w}(\mathbf{A}, \mathbf{B}) \in \mathbb{R}^I$  are given as

$$[\mathbf{w}(\mathbf{A}, \mathbf{B})]_i = \mathbf{b}_i^H \Psi_0(\mathbf{A}) \mathbf{b}_i, \quad (4)$$

where  $\Psi_0(\mathbf{A}) = \mathbf{I}$  if the baseband power shall be minimized as in [35], or  $\Psi_0(\mathbf{A}) = \mathbf{A}^H \mathbf{A}$  if the RF power shall be minimized as in, e.g., [31]. As we will see in Sec. III,  $\Psi_0$  serves a role similar to  $\Psi_i$  for  $i \neq 0$  in the equivalent virtual uplink system, where it represents the noise covariance. For ease of notation, we omit the arguments of  $\mathbf{w}$  in the following. Given a maximum total allocated power  $P_{\max}$ , the energy-efficient hybrid BF problem is formulated as

$$\begin{aligned} \min_{\mathbf{p}, \mathbf{A}, \mathbf{B}} \quad & \mathbf{w}^T \mathbf{p} \\ \text{s.t.} \quad & \mathbf{A} \in \mathcal{A}, \mathbf{B} \in \mathcal{B} \\ & \mathbf{w}^T \mathbf{p} \leq P_{\max}, \quad \mathbf{p} \geq 0, \\ & (\forall i) \text{SINR}_i^{\text{DI}}(\mathbf{p}, \mathbf{B}, \mathbf{A}) \geq \gamma_i, \end{aligned} \quad (5)$$

for which we define the set of possible analog beamformer matrices  $\mathbf{A}$  and baseband BF matrices  $\mathbf{B}$ , respectively, as

$$\begin{aligned} \mathcal{A} = \{ & [\mathbf{a}_1 \cdots \mathbf{a}_{M_{\text{rf}}}] \mid (\forall r \in \{1, \dots, M_{\text{rf}}\}) \mathbf{a}_r \in \mathcal{A}_{\text{rf}}, \\ & \text{rank}([\mathbf{a}_1 \cdots \mathbf{a}_{M_{\text{rf}}}] = M_{\text{rf}} \}, \quad (6) \\ \mathcal{B} = \{ & [\mathbf{b}_1 \cdots \mathbf{b}_I] \mid (\forall i \in \{1, \dots, I\}) \\ & \mathbf{b}_i \in \mathbb{C}^{M_{\text{rf}}} \wedge \|\mathbf{b}_i\|_2 = 1 \}. \quad (7) \end{aligned}$$

Note that in (6) we restrict  $\mathbf{A}$  to a selection of linearly independent codewords.

### C. Energy-efficient Hybrid Beamforming with Inexact CSI

Next, we assume that only inexact CSI

$$\hat{\mathbf{R}}_i = \mathbf{R}_i + \tilde{\mathbf{R}}_i, \quad (8)$$

is available at the transmitter, where  $\tilde{\mathbf{R}}_i \in \mathbb{C}^{M \times M}$  such that  $\hat{\mathbf{R}}_i \succeq \mathbf{0}$  is the CSI error resulting from, e.g., channel estimation error or feedback quantization. Furthermore, let  $\mathcal{P}(\mathcal{S})$  denote a probability distribution of system realizations  $\mathcal{S} = ((\mathbf{R}_i, \tilde{\mathbf{R}}_i, \gamma_i, \boldsymbol{\xi}_i)_{i=1}^I, P_{\max})$ , where  $\boldsymbol{\xi}_i$  denotes available auxiliary features that encode information about the characteristics of the CSI estimate. For instance,  $\boldsymbol{\xi}_i$  may represent the quantization level of the channel feedback or the pilot power used during channel sounding. Specific choices of  $\boldsymbol{\xi}_i$  are discussed in Sec. V. In addition, we define a mapping

$$\mathcal{M}(\mathcal{S}) = (\mathbf{p}_{\mathcal{M}}(\mathcal{S}), \mathbf{A}_{\mathcal{M}}(\mathcal{S}), \mathbf{B}_{\mathcal{M}}(\mathcal{S})) \quad (9)$$

where  $\mathbf{p}_{\mathcal{M}}(\mathcal{S})$ ,  $\mathbf{A}_{\mathcal{M}}(\mathcal{S})$  and  $\mathbf{B}_{\mathcal{M}}(\mathcal{S})$  are individual mappings from realizations  $\mathcal{S}$  onto the power allocation  $\mathbf{p}$ , the analog beamformers  $\mathbf{A}$  and digital precoders  $\mathbf{B}$ , respectively. Under the scenario distribution characterized by  $\mathcal{P}(\mathcal{S})$ , our aim is to find a mapping  $\mathcal{M}(\cdot)$  that, without accessing the ground-truth CSI  $\mathbf{R}_i$ , minimizes the expected allocated power while the QoS constraints  $\text{SINR}_i^{\text{DI}}(\mathcal{M}(\mathcal{S})) \geq \gamma_i$  are satisfied with probability  $1 - P_{\text{out}}$ , where  $P_{\text{out}}$  is a nominal outage probability. Given a mapping  $\mathcal{M}(\cdot)$ , satisfaction of this probabilistic QoS constraint is equivalent to non-positivity of

$$\begin{aligned} g_i(\mathcal{M}, \mathcal{P}(\mathcal{S})) \\ = 1 - P_{\text{out}} - \mathbb{P}_{\mathcal{S} \sim \mathcal{P}(\mathcal{S})} \left( \text{SINR}_i^{\text{DI}}(\mathcal{M}(\mathcal{S})) \geq \gamma_i \right), \quad (10) \end{aligned}$$

where the rightmost term is the non-outage probability. Note that both  $\text{SINR}_i^{\text{DI}}$  and  $\gamma_i$  implicitly depend on the realization  $\mathcal{S}$ . The desired robust energy-efficient hybrid BF problem, therefore, can be formulated as

$$\begin{aligned} \min_{\mathcal{M}} \quad & \mathbb{E}_{\mathcal{S} \sim \mathcal{P}(\mathcal{S})} (\mathbf{w}^T \mathbf{p}_{\mathcal{M}}(\mathcal{S})) \\ \text{s.t.} \quad & (\forall \mathcal{S} \in \text{supp}(\mathcal{P}(\mathcal{S}))) \begin{cases} \mathbf{A}_{\mathcal{M}}(\mathcal{S}) \in \mathcal{A} \\ \mathbf{B}_{\mathcal{M}}(\mathcal{S}) \in \mathcal{B} \\ \mathbf{p}_{\mathcal{M}}(\mathcal{S}) \geq \mathbf{0} \\ \mathbf{w}^T \mathbf{p}_{\mathcal{M}}(\mathcal{S}) \leq P_{\max} \end{cases} \quad (11) \\ & (\forall i) g_i(\mathcal{M}, \mathcal{P}(\mathcal{S})) \leq 0. \end{aligned}$$

Unlike QoS constraints based on *expected* values [55] or worst-case robust designs [15], outage constraints prevent extreme cases dominating the solution, thus ensuring that the majority of users achieve the target QoS level  $\gamma_i$ .

### III. Hybrid Downlink Beamforming and Power Allocation for Perfect CSI

Before considering robust energy-efficient hybrid BF using imperfect CSI, we first return to the exact CSI problem (5). In [35], an optimal and two sub-optimal algorithms are proposed to solve the optimization problem. While [35] only considers the case  $\mathbf{w} = \mathbf{1}$ , the generalization to (4) is straightforward.

The optimal algorithm evaluates the reduced  $M_{\text{rf}}$ -port digital BF subproblem with fixed  $\mathbf{A}$

$$\begin{aligned} \min_{\mathbf{p}, \mathbf{B}} \quad & \mathbf{w}^T \mathbf{p} \\ \text{s.t.} \quad & \mathbf{B} \in \mathcal{B}, \\ & \mathbf{w}^T \mathbf{p} \leq P_{\max}, \quad \mathbf{p} \geq 0, \\ & (\forall i) \text{ SINR}_i^{\text{Dl}}(\mathbf{p}, \mathbf{B}, \mathbf{A}) \geq \gamma_i, \end{aligned} \quad (12)$$

for each configuration  $\mathbf{A} \in \mathcal{A}$  (excluding equivalent configurations under permutation). While optimal, the growth in the number of configurations renders the optimal algorithm computationally impractical. Instead, we focus on the sub-optimal greedy correction algorithm in [35, Alg. 2]. Define

$$(\mathbf{p}^*(\Psi(\mathbf{A})), \mathbf{B}^*(\Psi(\mathbf{A}))) = \mathcal{F}_{\text{Dl}}(\Psi(\mathbf{A})) \quad (13)$$

with  $\Psi(\mathbf{A}) = (\Psi_i(\mathbf{A}))_i$  as the mapping onto the solution of the digital BF subproblem in (12) for some choice of  $\mathbf{A}$ . In each iteration  $\ell = 1, \dots, L_{\text{rf}}$  of the greedy correction algorithm, the idea is to select a particular analog RF chain  $r^{(\ell)} \in \{1, \dots, M_{\text{rf}}\}$  to update, then obtain  $\mathbf{A}^{(\ell)}$  as the correction

$$\mathbf{A}_{r^{(\ell)}}^{(\ell-1)} \left( \mathbf{a}_{r^{(\ell)}}^{(\ell)} \right) = \left[ \mathbf{a}_1^{(\ell-1)} \cdots \mathbf{a}_{r^{(\ell)-1}}^{(\ell-1)} \quad \mathbf{a}_{r^{(\ell)}}^{(\ell)} \quad \mathbf{a}_{r^{(\ell)+1}}^{(\ell-1)} \cdots \mathbf{a}_{M_{\text{rf}}}^{(\ell-1)} \right], \quad (14)$$

where the updated beam  $\mathbf{a}_{r^{(\ell)}}^{(\ell)}$  is chosen such that it minimizes the total allocated power, i.e.,  $\mathbf{a}_{r^{(\ell)}}^{(\ell)} = \check{\mathbf{a}}_{a^{(\ell)}}$  with

$$a^{(\ell)} = \arg \min_{a \in \{1, \dots, A\}} \mathbf{w}^T \mathbf{p}^* \left( \Psi \left( \mathbf{A}_{r^{(\ell)}}^{(\ell-1)}(\check{\mathbf{a}}_a) \right) \right). \quad (15)$$

Since  $\mathbf{w}^T \mathbf{p}^* \left( \Psi \left( \mathbf{A}^{(\ell)} \right) \right) \leq \mathbf{w}^T \mathbf{p}^* \left( \Psi \left( \mathbf{A}^{(\ell-1)} \right) \right)$  for any sequence of  $(r^{(\ell)})_\ell$  with feasible initialization, the algorithm converges.

The BF subproblem in (12) is established, and several algorithms are proposed in the literature to find a feasible solution [56]–[58]. Commonly, these algorithms are based on the dual virtual uplink problem [56]

$$\begin{aligned} \min_{\mathbf{q}, \mathbf{B}} \quad & \mathbf{1}^T \mathbf{q} \\ \text{s.t.} \quad & \mathbf{B} \in \mathcal{B} \\ & \mathbf{1}^T \mathbf{q} \leq P_{\max}, \quad \mathbf{q} \geq 0, \\ & (\forall i) \text{ SINR}_i^{\text{Ul}}(\mathbf{q}, \mathbf{B}, \mathbf{A}) \geq \gamma_i, \end{aligned} \quad (16)$$

where  $\mathbf{q} = [q_1 \ \cdots \ q_T]^T$  is the uplink power allocation and

$$\text{SINR}_i^{\text{Ul}}(\mathbf{q}, \mathbf{B}, \mathbf{A}) = \frac{q_i \mathbf{b}_i^H \Psi_i(\mathbf{A}) \mathbf{b}_i}{\sum_{j \neq i} q_j \mathbf{b}_i^H \Psi_j(\mathbf{A}) \mathbf{b}_i + \mathbf{b}_i^H \Psi_0(\mathbf{A}) \mathbf{b}_i} \quad (17)$$

is the virtual uplink SINR, to solve the problem efficiently. It is shown in, e.g., [56] or by slightly modifying the derivations in [58], that problem (12) is feasible if and only if problem (16) is feasible. Further, if optimal points exist, then the weighted downlink power and virtual uplink power at the optimum are equal ( $\mathbf{w}^T \mathbf{p}^* = \mathbf{1}^T \mathbf{q}^*$ ) and the optimal beamformers  $\mathbf{B}^*$  are identical. Consequently, it suffices to leverage the solution of (16)

$$(\mathbf{q}^*(\Psi(\mathbf{A})), \mathbf{B}^*(\Psi(\mathbf{A}))) = \mathcal{F}_{\text{Ul}}(\Psi(\mathbf{A})) \quad (18)$$

and update  $\mathbf{A}$  and  $\mathbf{B}$  according to<sup>1</sup>

$$\mathbf{A}^{(\ell)} = \mathbf{A}_{r^{(\ell)}}^{(\ell-1)}(\check{\mathbf{a}}_{a^{(\ell)}}), \quad (19)$$

$$\mathbf{B}^{(\ell)} = \mathbf{B}^* \left( \Psi \left( \mathbf{A}_{r^{(\ell)}}^{(\ell-1)}(\check{\mathbf{a}}_{a^{(\ell)}}) \right) \right), \quad (20)$$

$$\text{with } a^{(\ell)} = \arg \min_{a \in \{1, \dots, A\}} \mathbf{1}^T \mathbf{q}^* \left( \Psi \left( \mathbf{A}_{r^{(\ell)}}^{(\ell-1)}(\check{\mathbf{a}}_a) \right) \right). \quad (21)$$

Finally, utilizing  $\mathbf{B}^{(L_{\text{rf}})}$ , the downlink power allocation  $\mathbf{p}^*$  can be easily recovered by solving

$$\mathbf{C}_C(\mathbf{B}^{(L_{\text{rf}})}, \mathbf{A}^{(L_{\text{rf}})}) \mathbf{p}^* = \mathbf{1}, \quad (22)$$

where the coupling relationship is described by the matrix  $\mathbf{C}_C(\mathbf{B}, \mathbf{A}) \in \mathbb{R}^{I \times I}$  with [58]

$$[\mathbf{C}_C(\mathbf{B}, \mathbf{A})]_{i,j} = \begin{cases} \gamma_i^{-1} \mathbf{b}_i^H \Psi_i(\mathbf{A}) \mathbf{b}_i & \text{for } i = j. \\ -\mathbf{b}_j^H \Psi_i(\mathbf{A}) \mathbf{b}_j & \text{for } i \neq j, \end{cases} \quad (23)$$

In this work, we solve (16) by a variation of [58, Alg. 2] that replaces the unity uplink noise variance by the term  $\mathbf{b}_i^H \Psi_0(\mathbf{A}) \mathbf{b}_i$  resulting from weighting the downlink power.

#### IV. Robust Unrolled Hybrid Downlink Beamforming and Power Allocation

##### A. Proposed Model Architecture

We return to the case of imperfect CSI. Classical robust BF methods typically handle CSI uncertainty by explicit substitution of  $\mathbf{R}_i$  with  $\widehat{\mathbf{R}}_i - \widetilde{\mathbf{R}}_i$  in the QoS model. For the downlink SINR, for instance, this results in

$$\begin{aligned} & \widehat{\text{SINR}}_i^{\text{Dl}}(\mathbf{p}, \mathbf{B}, \mathbf{A}) \\ &= \frac{p_i (\mathbf{b}_i^H \mathbf{A}^H \widehat{\mathbf{R}}_i \mathbf{A} \mathbf{b}_i - \mathbf{b}_i^H \mathbf{A}^H \widetilde{\mathbf{R}}_i \mathbf{A} \mathbf{b}_i)}{\sum_{j \neq i} p_j (\mathbf{b}_j^H \mathbf{A}^H \widehat{\mathbf{R}}_i \mathbf{A} \mathbf{b}_j - \mathbf{b}_j^H \mathbf{A}^H \widetilde{\mathbf{R}}_i \mathbf{A} \mathbf{b}_j) + 1}. \end{aligned} \quad (24)$$

If the probability distribution of the error is assumed to be known and tractable, e.g., Gaussian or uniform, the probabilistic constraints can be translated into second-order cone or semidefinite constraints by finding suitable bounds of the error terms involving  $\widetilde{\mathbf{R}}_i$  (c.f. [13], [14]). Albeit these approaches control outage jointly across multiple users, the error distribution is typically not known in practice and the respective convex optimization problems incur a high computational cost. Alternatively, a computationally efficient approach for introducing robustness is to utilize a deterministic approximation  $\mathbf{E}_i \approx \widetilde{\mathbf{R}}_i$  of the error, e.g., diagonal loading [10]–[12]. Effectively, a *virtual* channel is considered. However, finding approximations that realize particular outage levels in MU systems and, at the same time, are efficient w.r.t. the allocated power is not straightforward.

We therefore propose a model-aided DN architecture  $\mathcal{M}(\mathcal{S}; \theta) = (\mathbf{p}_{\mathcal{M}}(\mathcal{S}; \theta), \mathbf{A}_{\mathcal{M}}(\mathcal{S}; \theta), \mathbf{B}_{\mathcal{M}}(\mathcal{S}; \theta))$  with parameters  $\theta$  based on the greedy correction algorithm [35, Alg. 2] that is reviewed in Sec. III. Inspired by the deterministic approximation approach, it leverages a dynamic GNN-based representation of  $\mathbf{E}_i$  that adapts to scenario instances, thus implicitly learning the error distribution from data.

<sup>1</sup>If  $\mathbf{A}_{r^{(\ell)}}^{(\ell-1)}(\check{\mathbf{a}}_a) \notin \mathcal{A}$ , we declare  $\mathbf{w}^T \mathbf{p}^* \left( \Psi \left( \mathbf{A}_{r^{(\ell)}}^{(\ell-1)}(\check{\mathbf{a}}_a) \right) \right) = \infty$ .

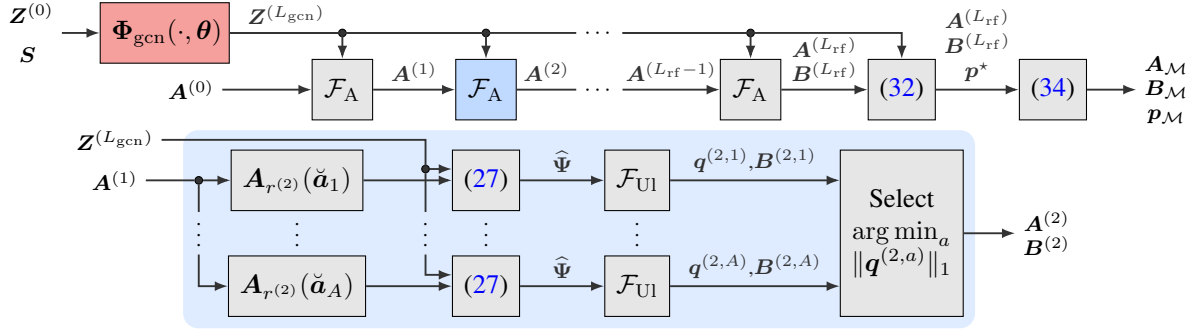


**FIGURE 2.** Block diagram of the proposed DN architecture  $\mathcal{M}(S; \theta)$  for outage-constrained hybrid BF.  $\mathcal{F}_A$  represent one analog beamformer selection step, while  $\mathcal{F}_{\text{UI}}$  represents solving the virtual uplink problem (31).

Specifically, we consider the QoS model

$$\widehat{\text{SINR}}_i^{\text{DI}}(\mathbf{p}, \mathbf{B}, \mathbf{A}) = \frac{p_i \mathbf{b}_i^H \widehat{\Psi}_{i,i}(\mathbf{A}) \mathbf{b}_i}{\sum_{j \neq i} p_j \mathbf{b}_j^H \widehat{\Psi}_{i,j}(\mathbf{A}) \mathbf{b}_j + 1}, \quad (25)$$

$$\widehat{\text{SINR}}_i^{\text{UI}}(\mathbf{q}, \mathbf{B}, \mathbf{A}) = \frac{q_i \mathbf{b}_i^H \widehat{\Psi}_{i,i}(\mathbf{A}) \mathbf{b}_i}{\sum_{j \neq i} q_j \mathbf{b}_j^H \widehat{\Psi}_{j,i}(\mathbf{A}) \mathbf{b}_i + \mathbf{b}_i^H \widehat{\Psi}_{0,i}(\mathbf{A}) \mathbf{b}_i}, \quad (26)$$

where positive semidefinite virtual channel covariances  $\widehat{\Psi}_{i,j}$  for  $i = 1, \dots, I$  and  $j = 1, \dots, I$  are given as

$$\widehat{\Psi}_{i,j}(\mathbf{A}) = \begin{cases} \mathbf{A}^H \begin{pmatrix} z_{i,1} \widehat{\mathbf{R}}_i + z_{i,2} \frac{\text{Tr}(\widehat{\mathbf{R}}_i)}{M} \mathbf{I} \\ z_{i,3} \widehat{\mathbf{R}}_i + z_{i,4} \frac{\text{Tr}(\widehat{\mathbf{R}}_i)}{M} \mathbf{I} \end{pmatrix} \mathbf{A} & \text{for } i = j, \\ \mathbf{A}^H \begin{pmatrix} z_{i,1} \widehat{\mathbf{R}}_i + z_{i,2} \frac{\text{Tr}(\widehat{\mathbf{R}}_i)}{M} \mathbf{I} \\ z_{i,3} \widehat{\mathbf{R}}_i + z_{i,4} \frac{\text{Tr}(\widehat{\mathbf{R}}_i)}{M} \mathbf{I} \end{pmatrix} \mathbf{A} & \text{for } i \neq j. \end{cases} \quad (27)$$

For  $i = 0$  we simply choose the original uplink noise covariance  $\widehat{\Psi}_{0,i}(\mathbf{A}) = \Psi_0(\mathbf{A})$ . The coefficients  $z_{i,1} > 0$  and  $z_{i,3} > 0$  model error components proportional to the quadratic forms  $\mathbf{b}_j^H \mathbf{A}^H \widehat{\mathbf{R}}_i \mathbf{A} \mathbf{b}_j$  in (24), i.e., the correlation between beamformers and channel estimates. The remaining coefficients  $z_{i,2} > 0$  and  $z_{i,4} > 0$  model error components that are independent of the spatial structure of the channel estimate and are only proportional to the gain  $\text{Tr}(\widehat{\mathbf{R}}_i)$ . Note that we allow separate error approximations for the wanted and interfering signals to account for the dependence on the beamformers  $\mathbf{b}_j$  of interfering users.

The coefficients matrix  $\mathbf{Z}_{\text{out}} \in \mathbb{R}^{I \times F_{\text{out}}}$  with  $F_{\text{out}} = 4$  and entries  $[\mathbf{Z}_{\text{out}}]_{i,f} = z_{i,f}$  representing the error components in (27) are estimated in an instance-adaptive manner by a graph convolutional neural network (GCN)  $\Phi_{\text{gcn}}(\cdot; \theta) : \mathbb{R}^{I \times F^{(0)}} \times \mathbb{R}^{I \times I} \rightarrow \mathbb{R}^{I \times F^{(L_{\text{gcn}})}}$  [59] with  $L_{\text{gcn}}$  layers, where  $F^{(0)} = F_{\text{in}}$  is the number of input features and  $F^{(L_{\text{gcn}})} = F_{\text{out}}$ . The transformation of latent features by the GCN  $\Phi_{\text{gcn}} = \check{\Phi}_{\text{gcn}}^{(L_{\text{gcn}})} \circ \dots \circ \check{\Phi}_{\text{gcn}}^{(1)}$  is characterized by the nonlinear map

$$\begin{aligned} \mathbf{Z}^{(\ell')} &= \check{\Phi}_{\text{gcn}}^{(\ell')}(\mathbf{Z}^{(\ell'-1)}, \mathbf{S}; \theta^{(\ell')}) \\ &= \phi^{(\ell')} \left( \sum_{f=0}^{F_{\text{gcn}}} \mathbf{S}^f \mathbf{Z}^{(\ell'-1)} \Theta_f^{(\ell')} + \mathbf{1} \left( \theta_b^{(\ell')} \right)^T \right), \end{aligned} \quad (28)$$

where  $\ell'$  is the GCN layer index,  $\phi^{(\ell')}$  is an elementwise nonlinearity,  $\theta^{(\ell')} = (\Theta_0^{(\ell')}, \dots, \Theta_{F_{\text{gcn}}}^{(\ell')}, \theta_b^{(\ell')})$  are learnable

weights with  $\Theta_f^{(\ell')} \in \mathbb{R}^{F^{(\ell'-1)} \times F^{(\ell')}}$  and  $\theta_b^{(\ell')} \in \mathbb{R}^{(\ell')}$ , and  $F_{\text{gcn}}$  is the filter degree. A GCN, which is a type of GNN, is a DN architecture tailored for graph-structured data. Each row  $[\mathbf{Z}^{(\ell')}]_{i,:}$  can be interpreted as the (latent) feature vector of a node of a graph, in this case, the users of the system. Here, the shift operator  $\mathbf{S}$  encodes the associated graph topology, specifically, the estimated correlation coefficient between channels of users

$$[\mathbf{S}]_{i_1, i_2} = \begin{cases} \frac{|\text{Tr}(\widehat{\mathbf{R}}_{i_1} \widehat{\mathbf{R}}_{i_2})|}{\|\widehat{\mathbf{R}}_{i_1}\|_F \|\widehat{\mathbf{R}}_{i_2}\|_F} & \text{for } i_1 \neq i_2, \\ 0 & \text{for } i_1 = i_2. \end{cases} \quad (29)$$

We define the input feature vector per user as

$$[\mathbf{Z}^{(0)}]_{i,:} = \left[ \log \|\widehat{\mathbf{R}}_i\|_F^2 \quad \log \gamma_i \quad \log \xi_i^T \quad \log P_{\text{max}} \right]^T. \quad (30)$$

On the one hand, the topology defined by the shift operator enables the GCN to predict the interference-related coefficients  $z_{i,3}$  and  $z_{i,4}$  associated with pairs of users. Compared to alternative DN architectures, GNNs, and thus GCNs by extension, have the advantage that they can be applied to similar graph-structured data with any number of nodes (users) given the same set of learnable weights [60]. Moreover, the mapping provided by GNNs is *permutation equivariant*, guaranteeing that if the input graph is permuted, i.e., the users are relabeled, the output does not change except for the same permutation [61]. This is a necessary property for resource allocation communication systems, where we expect that permutations of users or antennas should lead to corresponding permutations of the optimal resources. On the other hand, the input feature vector enables adaptation to the realization of the channel state, the CSI quality and the QoS requirements. The logarithmic mapping compresses the value range and facilitates generalization across different scales of input features.

The integration of the GCN into the greedy correction algorithm is illustrated in Fig. 2, thereby denoting one iteration of the analog beamformer selection as  $\mathcal{F}_A$ . In  $\mathcal{F}_{\text{UI}}$ , instead of solving Problem (16), we substitute  $\widehat{\text{SINR}}_i^{\text{UI}}$  into  $\text{SINR}_i^{\text{UI}}$  and omit the power constraint  $\mathbf{1}^T \mathbf{q} \leq P_{\text{max}}$ . In

particular, we solve

$$\begin{aligned} \min_{\mathbf{q} \geq \mathbf{0}, \mathbf{B} \in \mathcal{B}} \quad & \mathbf{1}^T \mathbf{q} \\ \text{s.t.} \quad & (\forall i) \widehat{\text{SINR}}_i^{\text{UL}}(\mathbf{q}, \mathbf{B}, \mathbf{A}) \geq \gamma_i, \end{aligned} \quad (31)$$

where  $\widehat{\text{SINR}}_i^{\text{UL}}$  is defined in (26). The downlink power allocation  $\mathbf{p}^*$  is recovered by solving

$$\widehat{\mathbf{C}}_C(\mathbf{B}^{(L_{\text{rf}})}, \mathbf{A}^{(L_{\text{rf}})}) \mathbf{p}^* = \mathbf{1}, \quad (32)$$

where  $\widehat{\mathbf{C}}_C(\mathbf{B}^{(L_{\text{rf}})}, \mathbf{A}^{(L_{\text{rf}})})$  is (23) with  $\widehat{\Psi}_{i,j}$  accordingly substituted for  $\Psi_i$ , i.e.,

$$[\widehat{\mathbf{C}}_C(\mathbf{B}, \mathbf{A})]_{i,j} = \begin{cases} \gamma_i^{-1} \mathbf{b}_i^H \widehat{\Psi}_{i,i}(\mathbf{A}) \mathbf{b}_i & \text{for } i = j. \\ -\mathbf{b}_j^H \widehat{\Psi}_{i,j}(\mathbf{A}) \mathbf{b}_j & \text{for } i \neq j. \end{cases} \quad (33)$$

Note that since  $\widehat{\Psi}$  is constant across iterations, as in [35, Alg. 2], the total allocated power is a decreasing sequence over iterations  $\ell$  if the initial point is feasible. Finally, to guarantee feasibility w.r.t. the power constraints,  $\mathbf{p}^*$  is projected onto the feasible set by

$$\mathbf{p}_{\mathcal{M}}(\mathcal{S}) = \frac{P_{\max}}{P_{\max} + [\mathbf{w}^T [\mathbf{p}^*]_0^\infty - P_{\max}]_0^\infty} [\mathbf{p}^*]_0^\infty, \quad (34)$$

where the notation  $[\mathbf{x}]_0^\infty$  indicates an elementwise projection onto the interval  $[0, \infty)$ .

### B. Initialization

A good initialization of the analog configuration  $\mathbf{A}^{(0)}$  is essential for the existence of a solution to the optimization in (31). Otherwise, the subproblems to select codewords  $\mathbf{a}_{r^{(\ell)}} = \check{\mathbf{a}}$  may be infeasible for any  $\check{\mathbf{a}} \in \mathcal{A}_{\text{rf}}$ . In this work, we utilize the heuristic

$$\left( \mathbf{a}_1^{(0)}, \dots, \mathbf{a}_{M_{\text{rf}}}^{(0)} \right) = M_{\text{rf}} \arg \max_{\check{\mathbf{a}} \in \mathcal{A}_{\text{rf}}} \sum_{i=1}^I \frac{\check{\mathbf{a}}^H \widehat{\mathbf{R}}_i \check{\mathbf{a}}}{\text{Tr}(\widehat{\mathbf{R}}_i)} \quad (35)$$

that effectively chooses the  $M_{\text{rf}}$  beams that maximize the SNR w.r.t. the sum of normalized channels.

### C. Model Gradient

End-to-end learning of the parameters  $\theta$  of the proposed model  $\mathcal{M}(\mathcal{S}; \theta)$  described in Sec. IV-A requires the Jacobian of the operators that compose the model, see Fig. 2. There are two significant obstacles. First, the beam selection in (19) is nondifferentiable. Secondly, the digital beamformers  $\mathbf{B}^*$  and power allocation  $\mathbf{p}^*$  result from nested optimization problems. Since these typically do not admit closed-form solutions, the gradient w.r.t.  $\widehat{\Psi}(\mathbf{A})$  is not easily computable.

#### 1) Beam Selection

An approximate partial derivative of the selected beam  $\mathbf{a}_{r^{(\ell)}}^{(\ell)}$  w.r.t. the trial uplink power allocations  $\mathbf{q}^{(\ell, a)} = \mathbf{q}^* \left( \widehat{\Psi}(\mathbf{A}_{r^{(\ell)}}^{(\ell-1)}(\check{\mathbf{a}}_a)) \right)$  can be obtained by smoothing (19) into the Softmin-selection [53], [62]

$$\mathbf{a}_{r^{(\ell)}}^{(\ell)} = \frac{\sum_{a=1}^A \check{\mathbf{a}}_a e^{-\beta_M \|\mathbf{q}^{(\ell, a)}\|_1 / q_{\min}^{(\ell)}}}{\sum_{a=1}^A e^{-\beta_M \|\mathbf{q}^{(\ell, a)}\|_1 / q_{\min}^{(\ell)}}}, \quad (36)$$

where  $\beta_M > 0$  is an annealing parameter controlling the trade-off between smoothness and bias of the gradient approximation. The softmin operator approaches the argmin selection as  $\beta_M \rightarrow \infty$ . Since the softmin operator is not scale-invariant, we propose an instance-adaptive normalization  $q_{\min}^{(\ell)} = \min_a \|\mathbf{q}^{(\ell, a)}\|_1$  to decouple the difference of exponents belonging to different analog BF codewords  $\check{\mathbf{a}}_a$  in (36) from the absolute scale of the allocated power.

A disadvantage of smoothing between analog beams, apart from primal infeasibility, is the increased correlation between the combined channels  $\widehat{\mathbf{R}}_i^{1/2} \mathbf{a}_{r^{(\ell)}}^{(\ell)}$ . The reduced spatial separability between users leads to ill-conditioned or infeasible BF problems. To avoid this undesired effect, we instead utilize a deterministic variant of the Straight-Through Gumbel-Softmax approach [63] during training. In the forward pass, analog beamformers  $\mathbf{a}_{r^{(\ell)}}^{(\ell)}$  are selected according to the argmin selection in (19). When computing the gradient in the backward pass, however, the partial derivatives  $d\mathbf{a}_{r^{(\ell)}}^{(\ell)} / d\mathbf{q}^{(\ell, a)}$  are based on the differentiable proxy in (36).

#### 2) Digital Uplink Beamforming Problem

Next, we consider the gradient of the digital uplink BF problem in (31), which is represented by  $\mathcal{F}_{\text{UL}}$  in Fig. 2. Specifically, we discuss the Jacobi matrix of the optimal point  $(\mathbf{q}^{(\ell, a)}, \mathbf{B}^{(\ell, a)})$  w.r.t. the arguments  $\underline{\psi} = (\widehat{\psi}_{i,j})_{i,j}$  with

$$\underline{\psi}_{i,j} = \left[ \text{vec}_d(\widehat{\Psi}_{i,j})^T \quad \text{vec}_{\text{re}}(\widehat{\Psi}_{i,j})^T \quad \text{vec}_{\text{im}}(\widehat{\Psi}_{i,j})^T \right]^T, \quad (37)$$

where the subscripts d, re and im indicate the diagonal, off-diagonal real and imaginary elements, respectively, thereby accounting for the Hermitian structure of virtual channel covariance  $\widehat{\Psi}_{i,j}$ . Efficient algorithms for solving Problem (31) in the case of general positive semidefinite (PSD) channels  $\widehat{\Psi}_{i,j}$  rely on cascaded eigendecompositions [58]. Since the derivative of the eigenvectors is undefined in case of repeated eigenvalues [64], a straightforward truncation and subsequent backpropagation through the underlying algorithm leads to numerical instability.

We therefore seek a method for obtaining the gradient that is independent of the underlying solver. Given a parameterized convex optimization problem with differentiable objective and constraint functions, under suitable regularity conditions (i.e., if strong duality holds), the optimal points are identifiable as the solution to the Karush-Kuhn-Tucker (KKT) conditions [65]. By summarizing the first-order stationarity condition, potential equality conditions and complementary slackness conditions of the KKT conditions as a real-valued system of nonlinear equations (SNLE)  $\mathbf{g}(\zeta, \underline{\psi}) = \mathbf{0}$ , where  $\zeta$  collects all primal and dual optimization variables, the implicit function theorem [66] can be applied to obtain the gradient if it exists. For these cases, automatic differentiation tools have been proposed [67], [68].

Applying such implicit differentiation to Problem (31) is not straightforward due to its nonconvexity. It is possible,

however, to resort to the established convex reformulation of its dual downlink problem that leverages the semidefinite relaxation of  $p_i \mathbf{b}_i \mathbf{b}_i^H = \check{\mathbf{b}}_i \check{\mathbf{b}}_i^H$  to  $\check{\mathbf{B}}_i$ , where  $\check{\mathbf{b}}_i = \sqrt{p_i} \mathbf{b}_i$  [69]:

$$\begin{aligned} \min_{(\check{\mathbf{B}}_i)_{i=1}^I} & \sum_{i=1}^I \text{Tr}(\widehat{\Psi}_{0,i} \check{\mathbf{B}}_i) \\ \text{s.t.} & (\forall i) \check{\mathbf{B}}_i \succeq \mathbf{0}, \\ & (\forall i) \gamma_i^{-1} \text{Tr}(\widehat{\Psi}_{i,i} \check{\mathbf{B}}_i) - \sum_{j \neq i} \text{Tr}(\widehat{\Psi}_{i,j} \check{\mathbf{B}}_j) \geq 1. \end{aligned} \quad (38)$$

The corresponding first-order stationary condition can be absorbed into the dual variables  $\Lambda_i$  for all  $i$ , that are associated with the PSD constraints in (38), as

$$\Lambda_i(\mathbf{q}, \underline{\psi}) = \widehat{\Psi}_{0,i} - \gamma_i^{-1} q_i \widehat{\Psi}_{i,i} + \sum_{j \neq i} q_j \widehat{\Psi}_{j,i}, \quad (39)$$

where the virtual uplink power  $q_i$  is the dual variable corresponding to the  $i$ th inequality constraint. Leaving dual feasibility implicit, i.e.,  $\Lambda_i(\mathbf{q}, \underline{\psi}) \succeq \mathbf{0}$  and  $q_i \geq 0$ , the KKT conditions thus furnish the following SNLE:

$$(\forall i) \mathbf{0} = \Lambda_i(\mathbf{q}, \underline{\psi}) \check{\mathbf{B}}_i, \quad (40)$$

$$(\forall i) 0 = q_i \left( 1 - \gamma_i^{-1} \text{Tr}(\widehat{\Psi}_{i,i} \check{\mathbf{B}}_i) + \sum_{j \neq i} \text{Tr}(\widehat{\Psi}_{i,j} \check{\mathbf{B}}_j) \right). \quad (41)$$

Albeit the implicit function theorem is now applicable if (40)-(41) is formulated in terms of real values, the semidefinite relaxation substantially inflates the number of variables and, as a consequence, the cost of computing the gradient. In the following, to mitigate this problem, we therefore reduce (40)-(41) into a suitable and more efficient representation. To begin with, note that if a solution  $(\check{\mathbf{B}}_i^*, q_i^*)_i$  to Problem (38) exists, where  $(q_i^*)_i$  are the corresponding dual variables, a solution with rank-1  $\check{\mathbf{B}}_i^*$  for all  $i$  can always be found [70, Th. 3.2]. As such, the following equivalence is straightforward to show using the KKT conditions in (40)-(41):

**Lemma IV.1.** *The point  $(\check{\mathbf{B}}_i^*, q_i^*)_i$  is a solution to Problem (38) for some  $\underline{\psi}$  if and only if  $(\check{\mathbf{b}}_i^*, q_i^*)_i$  with  $\check{\mathbf{B}}_i^* = \check{\mathbf{b}}_i^* (\check{\mathbf{b}}_i^*)^H$  is a dual feasible solution of the SNLE*

$$(\forall i) \mathbf{0} = \mathbf{g}_{b,i}(\check{\zeta}, \underline{\psi}) = \Lambda_i(\mathbf{q}, \underline{\psi}) \check{\mathbf{b}}_i, \quad (42)$$

$$(\forall i) 0 = g_{q,i}(\check{\zeta}, \underline{\psi}) = q_i \left( 1 - \gamma_i^{-1} \check{\mathbf{b}}_i^H \widehat{\Psi}_{i,i} \check{\mathbf{b}}_i + \sum_{j \neq i} \check{\mathbf{b}}_j^H \widehat{\Psi}_{i,j} \check{\mathbf{b}}_j \right). \quad (43)$$

Although (42)-(43) retrieve the original optimization variables, they also reintroduce the phase ambiguity of the optimal beamformers  $\mathbf{b}_i^*$  in Problem (31). Specifically, if  $(\check{\mathbf{b}}_i^*, q_i^*)_{i=1}^I$  is a solution to the digital BF problem, then  $(\check{\mathbf{b}}_i^* e^{j\phi_i}, q_i^*)_{i=1}^I$  is for arbitrary  $\phi_i \in [0, 2\pi)$ , resulting in a nonconvex solution set. The existence of an infinite number of distinct solutions in an arbitrary open neighborhood of a solution  $\zeta = \zeta^*$  to any differentiable SNLE  $\mathbf{g}(\zeta, \underline{\psi}) = \mathbf{0}$  implies that  $\det(D_\zeta \mathbf{g}(\zeta^*, \underline{\psi})) = 0$  [66, Corollary 7.8]. Since this property prevents the application of the implicit function theorem, we further modify the SNLE by i) restricting the

set of solutions, ii) formulating it in terms of real-values and iii) removing redundant equations.

First, we constrain the beamformer phase by setting  $[\Im(\check{\mathbf{b}}_i)]_{M_{\text{rf}}} = 0$  and subsequently define

$$\check{\zeta} = \begin{bmatrix} \check{\mathbf{b}}^T & \mathbf{q}^T \end{bmatrix}^T = \begin{bmatrix} \check{\mathbf{b}}_1^T & \cdots & \check{\mathbf{b}}_I^T & q_1 & \cdots & q_I \end{bmatrix}^T, \quad (44)$$

where  $\check{\mathbf{b}}_i = \begin{bmatrix} \Re(\check{\mathbf{b}}_i)^T & [\Im(\check{\mathbf{b}}_i)]_{-M_{\text{rf}}}^T \end{bmatrix}^T$  is the restricted real-valued beamformer. Secondly and thirdly, we define the real-valued SNLE

$$\mathbf{0} = \mathbf{g}(\check{\zeta}, \underline{\psi}) = \begin{bmatrix} \mathbf{g}_b(\check{\zeta}, \underline{\psi})^T & \mathbf{g}_q(\check{\zeta}, \underline{\psi})^T \end{bmatrix}^T, \quad (45)$$

with the upper SNLE corresponding to (42) with the imaginary part of the  $M_{\text{rf}}$ th element removed:

$$\begin{aligned} \mathbf{g}_b(\check{\zeta}, \underline{\psi}) &= \begin{bmatrix} \Re(\mathbf{g}_{b,1}(\check{\zeta}, \underline{\psi}))^T & [\Im(\mathbf{g}_{b,1}(\check{\zeta}, \underline{\psi}))]_{-M_{\text{rf}}}^T \\ \cdots & \Re(\mathbf{g}_{b,I}(\check{\zeta}, \underline{\psi}))^T & [\Im(\mathbf{g}_{b,I}(\check{\zeta}, \underline{\psi}))]_{-M_{\text{rf}}}^T \end{bmatrix}^T. \end{aligned} \quad (46)$$

The lower SNLE is identical to (43) and simply

$$\mathbf{g}_q(\check{\zeta}, \underline{\psi}) = \begin{bmatrix} g_{q,1}(\check{\zeta}, \underline{\psi}) & \cdots & g_{q,I}(\check{\zeta}, \underline{\psi}) \end{bmatrix}^T, \quad (47)$$

thereby treating the removed arguments  $[\Im(\check{\mathbf{b}}_i)]_{M_{\text{rf}}}$  as 0.

Let us now identify the function returning a normalized, real-valued and optimal primal-dual solution of Problem (31) with added constraints  $[\Im(\check{\mathbf{b}}_i)]_M = 0$  for all  $i$  as  $\mathbf{f}_{\text{UI}}(\underline{\psi}) = \check{\zeta}^*$ . In addition, we define the normalized primal-dual vector

$$\mathbf{f}_{\text{BN}}(\check{\zeta}) = \begin{bmatrix} \check{\mathbf{f}}_{\text{BN}}^T(\check{\mathbf{b}}_1) & \cdots & \check{\mathbf{f}}_{\text{BN}}^T(\check{\mathbf{b}}_I) & \mathbf{q}^T \end{bmatrix}^T \quad (48)$$

where  $\check{\mathbf{b}} = \check{\mathbf{f}}_{\text{BN}}(\check{\mathbf{b}}) = (\|\check{\mathbf{b}}\|_2)^{-1} \check{\mathbf{b}}$ . Before stating the main result, we make the following technical assumption.

**Assumption IV.1.** *The convex downlink BF problem in (38) has a unique solution  $(\check{\mathbf{B}}_i^*, q_i^*)_i$  with  $q_i^* > 0$  for all  $i$ .*

It can be easily observed from the dual problem in (31) that if  $\gamma_i > 0$  and the problem is feasible, then  $q_i > 0$ .<sup>2</sup>

**Theorem IV.2.** *Let  $\check{\zeta}^* = \mathbf{f}_{\text{UI}}(\underline{\psi})$  and  $\check{\zeta}^*$  such that  $\check{\zeta}^* = \mathbf{f}_{\text{BN}}(\check{\zeta}^*)$ . Under Assumption IV.1, the point  $\check{\zeta}^*$  is a dual feasible critical point of  $\mathbf{g}(\check{\zeta}, \underline{\psi})$ , the Jacobi matrix  $D_\zeta \mathbf{g}(\check{\zeta}^*, \underline{\psi})$  is full-rank and*

$$\begin{aligned} D_{\underline{\psi}_{i,j}} \mathbf{f}_{\text{UI}}(\underline{\psi}) &= \\ & - D_\zeta \mathbf{f}_{\text{BN}}(\check{\zeta}^*) \left( D_\zeta \mathbf{g}(\check{\zeta}^*, \underline{\psi}) \right)^{-1} D_{\underline{\psi}_{i,j}} \mathbf{g}(\check{\zeta}^*, \underline{\psi}). \end{aligned} \quad (49)$$

*Proof:* See Appendix B.

A detailed description of the involved Jacobi matrices  $D_{\underline{\psi}_{i,j}} \mathbf{g}(\check{\zeta}, \underline{\psi})$  and  $D_\zeta \mathbf{f}_{\text{BN}}(\check{\zeta})$  is relegated to Appendix A. Theorem IV.2 establishes  $\mathbf{g}(\check{\zeta}, \underline{\psi})$  as an admissible compact

<sup>2</sup>In practice, feasible instances of (38) typically have unique solutions since eigenspaces of nonzero eigenvalues are almost never identical between channels, and principal eigenvalues almost never have multiplicity greater than one. Even in those cases, slight channel perturbations could be added.

representation of Problem (31). Compared with a direct implicit function approach based on the KKT conditions (40)-(41) of the convexified BF optimization problem (38), the proposed derivative substantially reduces the dimension of the inverted Jacobi matrix from  $I(M_{\text{rf}}^2 + 1) \times I(M_{\text{rf}}^2 + 1)$  to  $2IM_{\text{rf}} \times 2IM_{\text{rf}}$ . Furthermore, Theorem IV.2 ensures the existence of the gradient provided a minor technical assumption, which is not necessarily the case when differentiating general convex optimization problems [67]. In practice, if the assumption is not met, e.g., when the problem is not feasible, we set the partial gradient to  $\mathbf{0}$ .

## D. Training

### 1) Empirical risk optimization

We optimize the DN model parameters  $\theta$  w.r.t. the objective of robust energy-efficient hybrid BF, as defined by Problem (11), using empirical risk minimization. While the power constraints are enforced by the projection (34) embedded in the DN architecture, an analogous projection is not applicable to the probabilistic QoS constraints. Instead, the constraint can be integrated into the loss function as a penalty by following a primal-dual optimization approach [71].

Introducing dual variables  $\lambda = [\lambda_1 \cdots \lambda_{D_c}]^T$  for  $D_c$  constraints, the empirical risk can be composed as the Lagrangian

$$J(\mathcal{D}, \theta, \lambda) = \widehat{\mathbb{E}}_{\mathcal{S} \sim \mathcal{D}}(\mathbf{w}^T \mathbf{p}_{\mathcal{M}}(\mathcal{S}; \theta)) + \sum_{d=1}^{D_c} \lambda_d \tilde{g}(\mathcal{D}_d, \theta), \quad (50)$$

where  $\mathcal{D}$  is a dataset of system instances  $\mathcal{S}$ . Here,  $\tilde{g}(\mathcal{D}_d, \theta)$  denotes a differentiable empirical approximation of the QoS constraint (10), which we discuss later in this section. We allow each constraint term to be evaluated on a non-overlapping subset  $\mathcal{D}_d \subseteq \mathcal{D}$ , where  $\mathcal{D} = \cup_{d=1}^{D_c} \mathcal{D}_d$ . This provides additional flexibility in enforcing fairness across heterogeneous data subsets in the implementation of the constraint by the model  $\mathcal{M}$ . For instance, if the data set contains “difficult” and “easy” instances  $\mathcal{S}$  that require high and low transmit power, respectively, the trained model  $\mathcal{M}(\cdot; \theta^*)$  might satisfy the nominal outage  $P_{\text{out}}$  on average over the entire data set, yet systematically violate the QoS requirement on the subset of difficult instances. Partitioning the data into appropriately chosen subsets mitigates this imbalance by allowing the constraint to be applied more uniformly across different types of instances.

The model parameters  $\theta$  are optimized by approaching the saddle point

$$\min_{\theta} \max_{\lambda \geq 0} J(\mathcal{D}, \theta, \lambda) \quad (51)$$

via stochastic gradient descent steps based on minibatches  $\tilde{\mathcal{D}} \subset \mathcal{D}$ . Thereby, we alternate between primal descent steps in the direction  $-\nabla_{\theta} J(\tilde{\mathcal{D}}, \theta, \lambda)$  and dual ascent steps in the direction  $\nabla_{\lambda} J(\tilde{\mathcal{D}}, \theta, \lambda)$  [71].

### 2) Differentiable Outage Constraints

We follow an approach inspired by soft-to-hard annealing [62] that we initially proposed in our preliminary work [53] to obtain a differentiable probabilistic constraint. In particular, we approximate  $g_i(\mathcal{M}, \mathcal{P}(\mathcal{S}))$  in (10) as

$$\begin{aligned} g_i(\mathcal{M}(\mathcal{S}), \mathcal{P}(\mathcal{S})) &= 1 - P_{\text{out}} \\ &\quad - \mathbb{E}_{\mathcal{S} \sim \mathcal{P}(\mathcal{S})} \left( u \left( \gamma_i^{-1} \text{SINR}_i^{\text{Dl}}(\mathcal{M}(\mathcal{S}, \theta), \mathcal{S}) - 1 \right) \right) \\ &\approx 1 - P_{\text{out}} \\ &\quad - \frac{1}{I} \sum_i \widehat{\mathbb{E}}_{\mathcal{S} \sim \mathcal{D}} \left( \tilde{u}_{\beta_c} \left( \gamma_i^{-1} \text{SINR}_i^{\text{Dl}}(\mathcal{M}(\mathcal{S}, \theta), \mathcal{S}) - 1 \right) \right) \\ &= \tilde{g}_{\beta_c}(\mathcal{D}, \theta), \end{aligned} \quad (52)$$

where the non-outage probability is first expressed in terms of an expectation as well as the unit step function  $u(\cdot)$ , then approximated by the empirical mean and the differentiable logistic function  $\tilde{u}_{\beta_c}(x) = (1 + \exp(-\beta_c x))^{-1}$ . The parameter  $\beta_c$  controls the approximation of the unit step. To ensure meaningful gradients for arbitrary QoS violations,  $\beta_c$  is adapted by exponential averaging with step size  $\eta_c$  in each training step  $\tau$ , i.e.,

$$\begin{aligned} \beta_c^{(\tau)} &= (1 - \eta_c) \beta_c^{(\tau-1)} \\ &\quad + \frac{\eta_c}{\left[ -\widehat{\mathcal{Q}}_{\mathcal{S} \sim \mathcal{D}} \left( \gamma_i^{-1} \text{SINR}_i^{\text{Dl}}(\mathcal{M}(\mathcal{S}, \theta^{(\tau)})) - 1; P_{\text{out}} \right) \right]_{\beta_c^{-1}}^{\infty}}, \end{aligned} \quad (53)$$

where  $\widehat{\mathcal{Q}}_{\mathcal{S} \sim \mathcal{D}}(f(\mathcal{S}); p)$  denotes the empirical  $p$ -quantile of  $f(\mathcal{S})$  based on data set  $\mathcal{D}$ . As the outage probability decreases to the nominal value  $P_{\text{out}}$ , the empirical quantile in (53) approaches 0, thus  $\tilde{u}_{\beta_c}(\cdot)$  approaches the step function until the upper bound  $\beta_c = \bar{\beta}_c > 0$ . If the constraint is oversatisfied,  $\beta_c$  converges to  $\bar{\beta}_c$  as well. Compared to [49], for instance, where the smoothing parameter  $\beta_c$  is fixed, the proposed adaptive approach more accurately approximates the original outage constraint, e.g., at the end of training, while simultaneously obtaining informative gradients if the constraint is significantly violated, e.g., at the start of training. As a result, more “difficult” SINR requirements are realizable.

The resulting gradient also differs from that of the conventional quantile-based approach for empirical risk minimization [72]. The quantile-based approach, as adopted in [47], [48], [50] for wireless QoS constraints, approximates the QoS constraint directly by the empirical quantile:

$$\tilde{g}(\mathcal{D}, \theta) = \widehat{\mathcal{Q}}_{\mathcal{S} \sim \mathcal{D}} \left( \gamma_i - \text{SINR}_i^{\text{Dl}}(\mathcal{M}(\mathcal{S}, \theta)); 1 - P_{\text{out}} \right). \quad (54)$$

This quantile is positive whenever the empirical outage probability exceeds the nominal outage and negative if the QoS requirement is met with a margin. Here, the gradient depends only on the interpolated samples closest to the value of the empirical quantile [72]. In comparison, although our adaptive annealing approach introduces two hyperparameters  $\eta_c$  and  $\bar{\beta}_c$ , it has the crucial advantage to construct the gradient by averaging more samples of  $\text{SINR}_i^{\text{Ul}}$ , thereby

smoothing the loss surface. We empirically compare the performance of both approaches in Sec. V-C.

### 3) Convergence Metric

Model convergence is evaluated based on validation data  $\mathcal{D}_{\text{val}}$ . Over the course of training, the sequence of empirical loss values in (50) is not expected to be minimized near a saddle point because the dual updates continually reshape the objective landscape. Nevertheless, a quantitative criterion for convergence is crucial to compare training runs and methods. Therefore, we leverage the metric

$$J_{\text{cm}}^{(\tau)} = \frac{1}{I} \widehat{\mathbb{E}}_{\mathcal{S} \sim \mathcal{D}_{\text{val}}} \left( \mathbf{w}^T \mathbf{p}_{\mathcal{M}}(\mathcal{S}; \boldsymbol{\theta}^{(\tau)}) \right) + \sum_{d=1}^{D_c} \bar{\lambda}_d \left[ \widehat{g} \left( \mathcal{M}(\cdot; \boldsymbol{\theta}^{(\tau)}), \mathcal{D}_{\text{val},d} \right) \right]_0^\infty, \quad (55)$$

where  $\widehat{g}$  is the empirical estimate of the constraint in (10) on the subset  $\mathcal{D}_{\text{val},d}$  and averaged across users  $i$ , while  $\bar{\lambda}_d$  is an upper bound of  $\lambda_d$ . Negative values of  $\widehat{g}$  are projected to 0 to avoid rewarding constraint oversatisfaction. Since all constraints other than the QoS constraints are implicitly guaranteed by the model architecture of  $\mathcal{M}$ ,  $J_{\text{cm}}^{(\tau)}$  is an upper bound of the Lagrangian function belonging to Problem (11) given  $\lambda_d \leq \bar{\lambda}_d$ . The bound is tight if the QoS constraints are exactly met.  $J_{\text{cm}}^{(\tau)}$  is similar to the loss function of a penalty-based approach [49].

Primal and dual step sizes are decayed once by  $\eta_a$  if the sequence  $(J_{\text{cm}}^{(\tau_{\text{val}} \kappa)})_\kappa$  over training steps  $\tau = \tau_{\text{val}} \kappa$ , where  $\tau_{\text{val}}$  is the validation interval, does not improve to a new minimum within a window of length  $\tau_{\text{pat},1}$ . A run is considered converged if no improvement occurs within a window of length  $\tau_{\text{pat},2}$ .

## E. Discussion and Limitations

Compared to [35, Alg. 2] for perfect CSI, the additional computational cost by the proposed DN for imperfect CSI, that stems from the the instance-adaptive channel mapping, is marginal. During validation, the cost remains dominated by the optimization of the low-dimensional digital beamformers  $\mathbf{B}^{(\ell,a)}$  across the CB. With the reasonable assumption  $I < M_{\text{rf}}$ , a complexity  $\mathcal{O}(L_{\text{ul}} I M_{\text{rf}}^3)$  for solving (31), where  $L_{\text{ul}}$  accounts for iterations of the nested optimization, and ignoring the cost incurred by projections using the analog beams  $\check{\mathbf{a}}_i$ , this computational complexity scales according to  $\mathcal{O}(L_{\text{rf}} L_{\text{ul}} A I M_{\text{rf}}^3)$ . As such, while the codebook-based hybrid architecture allows for significant design flexibility, it is traded with computational cost that scales linearly in  $L_{\text{rf}} \geq M_{\text{rf}}$  and  $A$ . Similarly, since the cost of the gradient computation during training is dominated by the inversion required by Thm. IV.2, its computational complexity is  $\mathcal{O}(L_{\text{rf}} A I^3 M_{\text{rf}}^3)$ . Due to the implicit differentiation, however, only the result of each instance of the digital BF subproblem needs to be stored in memory instead of all intermediate results of the solver utilized for the subproblem.

Furthermore, we do not make assumptions on the distribution of the CSI error. Instead, the network learns both the effect of the CSI error as well as its relation to the feature  $\boldsymbol{\xi}$  during training. In this way, the design preserves the modular architecture of wireless systems by being agnostic to the CSI acquisition and feedback mechanism, unlike end-to-end joint estimation and BF schemes such as the one in [73]. Therefore, the proposed method is suitable for both MU time domain duplex and frequency domain duplex systems, with CSI feedback compression being a major source of error in the latter. In addition, the proposed architecture inherits support for the usage of both statistical and instantaneous CSI.

There are two main limitations regarding the training procedure. First, during training, the loss function requires access to accurate CSI to determine the outage, which can be challenging when working with real-world data. However, the data-efficiency and strong generalization capability of the model-aided DN approach help mitigating the problem. Secondly, the feasibility of the training data must be carefully considered. If an outage constraint renders the problem infeasible for the given combination of data and model architecture, e.g., if the set nominal outage is too low given the number of users, nominal SINR, or CSI uncertainty, then the corresponding dual variable grows unbounded and the training diverges. As such, the composition of the training data set must be designed with particular care. During testing, however, if the inner baseband problem (31) is infeasible for a system realization, e.g., if (32) yields negative power allocations, a failure to satisfy the QoS constraints is clearly indicated. In these cases, the problem instance could be relaxed by, e.g., rescheduling users to another resource block [36].

## V. Empirical Results

### A. Experimental Setup

The proposed architecture, training and experiments are implemented using PyTorch. To promote reproducibility, our code is published at <https://github.com/lsky96/outage-constrained-hybrid-bf-md-dnn>.

#### 1) Training

DN parameters are learned with minibatch stochastic gradient descent and the primal gradients are normalized using Adam with weight decay [74]. We employ 5-fold cross-validation and results are given as mean  $\pm$  standard deviation. To prevent convergence problems due to sporadic gradient explosion, we employ adaptive gradient clipping [75]. Specifically, we clip the  $\infty$ -norm of the primal gradient  $\|\nabla_{\boldsymbol{\theta}} J\|_\infty$  to a maximum of the current 0.90-quantile of the gradient norm history. Unless stated otherwise, the training parameters are summarized in Tab. 1 and the loss function in (50) with the annealing-based constraint in (52) are utilized. Pseudocode of the training procedure using the proposed annealing-based constraint is provided in Appendix C. We

**TABLE 1.** Parameters used for training, model configuration and data.

Training Param.	Symbol	Value
Adam smoothing		(0.9, 0.99)
Adam weight decay		0.1
primal step size	$\eta_p$	0.0005
dual step size	$\eta_d$	0.1 (0.002 for (54))
step size decay	$\eta_a$	0.2
minibatch size	$ \mathcal{D} $	200 (10 in Sec V-E)
anneal. constraint	$(\bar{\beta}_c, \eta_c)$	(50, 0.01)
validation interval	$\tau_{\text{val}}$	100
dual upper bound	$\bar{\lambda}_d$	100
stop. crit. patience	$(\tau_{\text{pat},1}, \tau_{\text{pat},2})$	(5000, 10000)
# train. instances	$ \mathcal{D}_{\text{train}} $	20000
# valid. instances	$ \mathcal{D}_{\text{val}} $	5000
Model Param.	Symbol	Value
# greedy selections	$L_{\text{rf}}$	$M_{\text{rf}}$
beam annealing	$\beta_M$	5
GCN param.	$(L_{\text{gcn}}, F_{\text{gcn}}, F^{(\ell)})$	(3, 1, 32)
coefficient bound	$\bar{\beta}_0$	8
Data Param.	Symbol	Value
Tx Antenna Dim.	$(M_x, M_y)$	(4, 4)
angular direction	$(\varphi_{x,i}, \varphi_{y,i})$	$\in [-60^\circ, 60^\circ] \times [-60^\circ, 30^\circ]$
angular spread	$\sigma_{\text{as}}$	$10^\circ$ ( $5^\circ$ in Sec. E)
max. Tx power	$P_{\text{max}}$	20 dB
minimum SINR	$\gamma_i$	$\in [5\text{dB}, 15\text{dB}]$
# RF chains	$M_{\text{rf}}$	5
nominal outage	$P_{\text{out}}$	0.1

remark that we found in empirical experiments that different choices of  $\bar{\lambda}_d$  do not significantly impact the final model performance as long as  $\bar{\lambda}_d$  is chosen as an upper bound of the dual variables.

## 2) Configuration of the proposed method

For the proposed architecture in Sec. IV-A, which we henceforth denote as *U-G-HBF-GCN*, we utilize  $L_{\text{gcn}}$ -layer GCNs of degree  $F_{\text{gcn}} = 1$ , where the nonlinear activation functions  $\phi^{(\ell)}$  are ReLU, except for the final layer where  $\phi^{(L_{\text{gcn}})}(x) = e^{\bar{\beta}_o \tanh(x/\bar{\beta}_o)}$  is an exponential with soft bounds  $[e^{-\bar{\beta}_o}, e^{\bar{\beta}_o}]$  [76]. The input features are normalized by a batchnorm layer [77]. A constant annealing parameter  $\beta_M$  is chosen in (36) for simplicity.

## 3) Benchmark methods

We compare to four approaches:

- *G-HBF-perf* is the greedy hybrid BF algorithm [35, Alg. 2] with  $L_{\text{rf}} = 2M_{\text{rf}}$  selections and perfect CSI.
- *G-HBF-marg* is the greedy hybrid BF algorithm [35, Alg. 2] accessing imperfect CSI with SINR target  $\gamma'_i = \gamma_i + \check{\gamma}$ , where  $\check{\gamma}$  is bisected until the nominal outage  $P_{\text{out}}$  is approximately attained on the validation data.
- *U-G-HBF-FCN* is similar to U-G-HBF-GCN, but uses only a GCN of degree  $F_{\text{gcn}} = 0$  with increased  $F^{(\ell)} = 64$ , which is equivalent to parallel fully connected DNs for each user.

- *U-FDBF-GCN* is a fully-digital version of U-G-HBF-GCN, where  $\mathbf{A} = \mathbf{I}$  effectively.

Both G-HBF-perf and U-FDBF-GCN serve as bounds that cannot be achieved without full CSI or per-antenna RF chains at the transmitter, respectively.

## 4) Data Generation

For each system instance  $\mathcal{S}$ , we generate channel covariance matrices  $\mathbf{R}_i = \mathbf{R}_{x,i} \otimes \mathbf{R}_{y,i} \in \mathbb{C}^{M \times M}$  with  $M = M_x M_y$  of a 2D uniform planar array with half-wavelength antenna distance. The covariance matrices  $\mathbf{R}_{x,i} \in \mathbb{C}^{M_x \times M_x}$  and  $\mathbf{R}_{y,i} \in \mathbb{C}^{M_y \times M_y}$  of both axes follow the spatial correlation model in [78] with uniformly sampled angular directions  $(\varphi_{x,i}, \varphi_{y,i})$  of user  $i$ . Instantaneous channel vectors are then sampled as  $\mathbf{h}_i \sim \mathcal{CN}(\mathbf{0}, \mathbf{R}_i)$ . We remove instances that are infeasible under perfect CSI.

We subsequently degrade the CSI in two ways:

- *Noisy MMSE estimator model*: We follow [12] and use

$$\hat{\mathbf{h}}_i = \mathbf{R}_i \left( \mathbf{R}_i + P_{\text{pil},i}^{-1} \mathbf{I} \right)^{-1} \left( \mathbf{h}_i + \sqrt{P_{\text{pil},i}}^{-1} \mathbf{n}_i \right), \quad (56)$$

where  $\mathbf{n}_i \sim \mathcal{CN}(\mathbf{0}, \mathbf{I})$  and  $P_{\text{pil},i} = \xi_i$  is the power of the pilot signal. For simplicity, the MMSE estimate accesses the true covariance.

- *DFT feedback quantization model*:  $\hat{\mathbf{h}}_i$  is obtained by 2D discrete Fourier transform (DFT) CB feedback quantization with  $N_{\text{fb}} = \xi_i$  feedback vectors modeled after the 3GPP 5G Type II codebook [79], [80], but restricted to a narrowband and unpolarized setting. The channel  $\mathbf{h}_i$  is first transformed by a  $2 \times 2$ -times oversampled 2D DFT. For each set of DFT-coefficients corresponding to one of the 4 orthogonal DFT vector subsets of the oversampled 2D-DFT, the top  $N_{\text{fb}}$  coefficients are quantized in 3 dB magnitude steps and 8-PSK phase steps.  $\hat{\mathbf{h}}_i$  is obtained by applying the IDFT to the top  $N_{\text{fb}}$  quantized coefficients of the oversampled vector subset that minimizes  $\|\hat{\mathbf{h}}_i\|_2$ .

The system instances  $\mathcal{S}$  are divided into  $D_c$  constraint groups as explained in Sec. IV-D, depending on the degradation  $\xi_i$ , i.e.,  $\xi_i$  is scalar.

## 5) Transmit codebook

The transmit CB  $\mathcal{A}_{\text{rf}}$  is a 2D-DFT CB without oversampling, leading to a size  $A = M$  [41], [79].

## B. Comparison between Methods

We construct datasets according to the parameters summarized in Tab. 1 with CSI degradation through noisy MMSE estimation with pilot power  $P_{\text{pil},i} = \xi_i$ . The data is subdivided into 4 constraint groups with  $\xi_i = 10\text{dB}$ ,  $\xi_i = 17\text{dB}$ ,  $\xi_i = 24\text{dB}$  and  $\xi_i$  uniformly distributed over  $[10\text{ dB}, 24\text{ dB}]$ , respectively. We remark that for this setup, on a machine with Arch Linux and AMD Epyc 9554P CPU limited to 3 threads, the proposed U-G-HBF-GCN has a runtime of

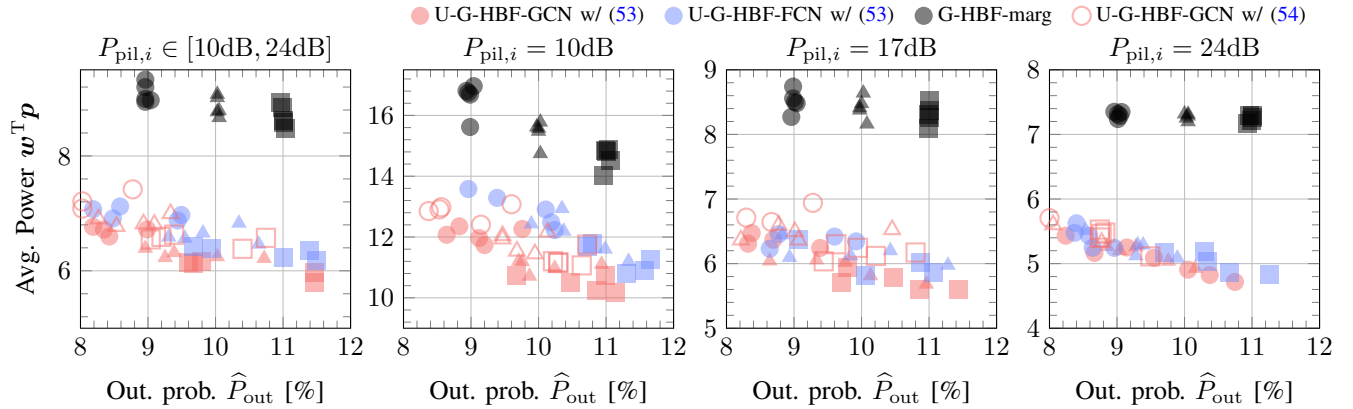


FIGURE 3. Allocated power over empirical outage probability for different targets  $P_{\text{out}}$ : 0.09 (circles), 0.10 (triangles), 0.11 (squares). 5 folds each.

TABLE 2. Results for  $M = 4 \times 4$  antennas with 3 users for nominal outage  $P_{\text{out}} = 0.10$  for CSI degradation based on different  $P_{\text{pil},i}$ .

Methods	$P_{\text{pil},i} \in [10\text{dB}, 24\text{dB}]$		$P_{\text{pil},i} = 10\text{dB}$		$P_{\text{pil},i} = 17\text{dB}$		$P_{\text{pil},i} = 24\text{dB}$	
	$\ \mathbf{p}\ _1$	$\hat{P}_{\text{out}} [\%]$	$\ \mathbf{p}\ _1$	$\hat{P}_{\text{out}} [\%]$	$\ \mathbf{p}\ _1$	$\hat{P}_{\text{out}} [\%]$	$\ \mathbf{p}\ _1$	$\hat{P}_{\text{out}} [\%]$
G-HBF-perf	$6.61 \pm 0.10$	$0.00 \pm 0.00$	$6.62 \pm 0.17$	$0.00 \pm 0.00$	$6.62 \pm 0.11$	$0.00 \pm 0.00$	$6.70 \pm 0.04$	$0.00 \pm 0.00$
G-HBF-marg	$8.86 \pm 0.17$	$10.03 \pm 0.01$	$15.44 \pm 0.40$	$10.00 \pm 0.00$	$8.41 \pm 0.17$	$10.01 \pm 0.04$	$7.27 \pm 0.05$	$10.03 \pm 0.02$
U-G-HBF-FCN	$6.62 \pm 0.14$	$9.93 \pm 0.55$	$12.07 \pm 0.69$	$10.59 \pm 0.57$	$6.17 \pm 0.18$	$9.86 \pm 1.03$	$5.26 \pm 0.17$	$9.28 \pm 0.49$
U-G-HBF-GCN	$6.28 \pm 0.07$	$9.67 \pm 0.70$	$11.04 \pm 0.20$	$10.10 \pm 0.51$	$5.92 \pm 0.17$	$9.77 \pm 0.87$	$5.14 \pm 0.15$	$9.42 \pm 0.54$
U-FDBF-GCN	$3.98 \pm 0.07$	$9.55 \pm 0.75$	$6.04 \pm 0.15$	$9.90 \pm 0.78$	$3.83 \pm 0.13$	$9.64 \pm 0.89$	$3.45 \pm 0.00$	$9.49 \pm 0.02$
U-G-HBF-GCN w/ (54)	$6.86 \pm 0.09$	$8.83 \pm 0.43$	$11.83 \pm 0.32$	$9.74 \pm 0.30$	$6.47 \pm 0.10$	$9.10 \pm 0.83$	$5.61 \pm 0.17$	$8.04 \pm 0.44$

$1.9 \pm 0.4$ ms per system realization, while one training step has a runtime of approximately 1 s.

The proposed and benchmark methods are compared in Fig. 3 and Tab. 2. To observe trends in the power-outage trade-off, we train models for nominal outage probabilities  $P_{\text{out}}$  of 0.09, 0.10 and 0.11, respectively. The proposed learning-based methods significantly outperform the benchmark G-HBF-marg. Moreover, U-G-HBF-GCN outperforms U-G-HBF-FCN, particularly if  $P_{\text{pil},i} = 10$  dB or if  $P_{\text{pil},i}$  is uniformly distributed over [10 dB, 24 dB]. This demonstrates the efficacy of the GNN-based approach, which leverages the similarity between channels of different users. The performance of the methods converge as the CSI quality improves, i.e., as the  $P_{\text{pil},i}$  increases, which is expected. Since a nonzero outage is targeted, the learning-based methods may allocate less power than G-HBF-perf. The fully-digital U-FDBF-GCN achieves a significantly better power-outage trade-off due to the number of RF chains of U-G-HBF-GCN, as will be seen in Sec. V-D. Notably, we find that the proposed DN models reliably generalize between different levels of CSI degradation, matching  $P_{\text{out}}$  in most cases within 1%, thereby demonstrating the effectiveness of multiple constraints and side-information  $\xi_i$ .

### C. Comparison to Quantile-based Constraint

We compare our proposed adaptive annealing-based constraint in (52) to the quantile-based penalty in [47], [48], [50], [72] with the U-G-HBF-GCN model. Since the dual

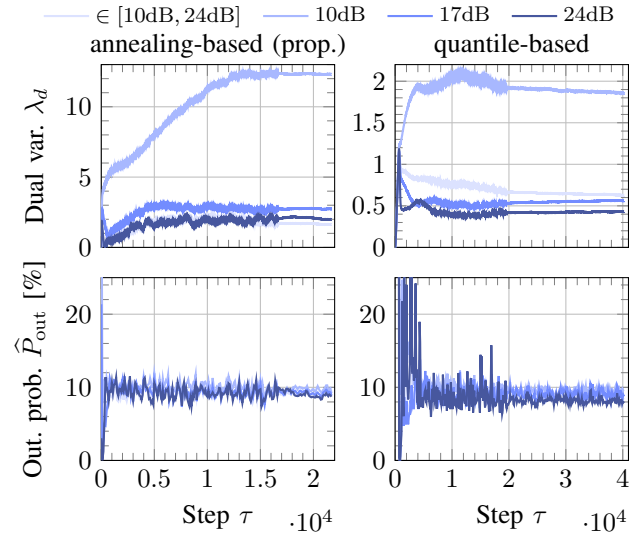


FIGURE 4. Empirical outage probability (validation) and dual variables corresponding to data groups of different CSI quality  $\xi_i = P_{\text{pil},i}$  for the training run of fold 1. Nominal outage  $P_{\text{out}} = 0.1$ .

variables and dual gradients have different scales, we adjust the dual step size  $\eta_d$ , see Tab. 1.

We observe in Fig. 3 and Tab. 2 that the proposed annealing-based constraint yields a slightly better power-outage trade-off, whereas the quantile-based method overfulfills the outage constraint for  $P_{\text{pil},i} = 24$  dB. Fig. 4 reveals the reason. Although the relative per-step changes in the dual variables are similar for both methods, the empirical outage

probability on the validation data exhibits substantially larger variability for the quantile-based approach, particularly at  $P_{\text{pil},i} = 24\text{dB}$ , which corresponds to the “easiest” constraint to satisfy. Note that the different constraint variants converge to distinct values of  $\lambda_d$  due to differences in the scaling of the associated constraint gradient. We hypothesize that the smoother loss landscape induced by instance averaging in the annealing-based constraint reduces the gradient variance across different data subsets. This also leads to faster training with  $(26 \pm 9) \cdot 10^3$  steps required for convergence compared to  $(34 \pm 8) \cdot 10^3$ , averaged over 15 runs.

Note that the sensitivity of the proposed adaptive constraint w.r.t. the value of its hyperparameters is empirically low. We do not observe a significant difference in model performance when changing the smoothing factor  $\eta_c$  to 0.002 and 0.05. Thereby,  $(29 \pm 7) \cdot 10^3$  and  $(26 \pm 6) \cdot 10^3$  training steps are taken until convergence. Similarly, increasing the annealing parameter bound  $\bar{\beta}_c$  from 50 to 250 does not significantly impact performance. However, reducing  $\bar{\beta}_c$  to 10 leads to overfulfillment of the outage constraints by 1.7% on average, indicating that the approximation of the outage in (52) is not sufficiently close at this value.

#### D. Generalization w.r.t. Number of Users

In this experiment, we investigate the domain adaptation capability of the integrated GNNs. For this, the number of users is randomly sampled from one to four in each training step  $\tau$ . Simultaneously, the number of constraints is quadrupled to 16 compared to Sec. V-B.

We present the results in Tab. 3 for  $M_{\text{rf}} = 8$ . Clearly, a single U-G-HBF-GCN model reliably achieves the nominal outage probability within a small error for systems with one to four users and both low and high CSI quality, thus demonstrating an excellent domain adaptation capability. An exception are single-user systems with  $P_{\text{pil},i} = 24\text{dB}$ , where the outage constraint is overfulfilled. The benchmark G-HBF-marg is again substantially outperformed, and the allocated power is close to G-HBF-perf if  $P_{\text{pil},i}$  is high. We are further interested in extrapolation performance if the tested user count is not contained in the training data set. U-G-HBF-GCN\* in Tab. 3 denotes models that are trained with only systems of two or three users. While the achieved power-outage trade-off for two or three users is similar to that of U-G-HBF-GCN, we observe comparable performance for one or four users at  $P_{\text{pil},i} = 24\text{dB}$ . When extrapolating to the most challenging case among the tested, four users and  $P_{\text{pil},i} = 10\text{dB}$ , the outage of U-G-HBF-GCN\* only degrades to  $15.94\% \pm 1.23\%$ . This generalization performance can be attributed to our use of a GCN, which is permutation-equivariant w.r.t. the users and, due to its parametrization, allows seamless application to arbitrary user counts and shift operator dimensions. Compared to Sec. V-B, hybrid BF now achieves performance close to fully digital BF, except for the case of 4 users. This occurs at the established threshold  $M_{\text{rf}} = 2I$ , which likewise applies to

hybrid BF architectures with more general phase shifting networks [7, Prop. 2].

#### E. Combined Statistical & Instantaneous CSI

Finally, we increase  $M$  to  $8 \times 8$ ,  $M_{\text{rf}}$  to 16 and sample  $\gamma_i$  in the interval [10dB, 20dB]. In addition, we consider DFT quantization with  $D_c = 4$  groups, where  $N_{\text{fb}} = 4$ ,  $N_{\text{fb}} = 6$ ,  $N_{\text{fb}} = 8$  and  $N_{\text{fb}} \in \{4, \dots, 8\}$  uniformly, respectively.

Furthermore, for each system instance  $\mathcal{S}$ , we sample 32 instantaneous channel coefficients  $(\mathbf{h}_{i,s})_{s=1}^{32}$  and compute  $\hat{\mathbf{R}}_i$  as the covariance estimate of  $(\hat{\mathbf{h}}_{i,s})_{s=1}^{32}$ . The estimated statistical CSI  $(\hat{\mathbf{R}}_i)_i$  is used to choose the analog beamforming matrix  $\mathbf{A}$ , while an additional uplink problem  $\mathcal{F}_{\text{UI}}$  is solved to obtain digital precoders  $\mathbf{B}$  for each corresponding sampled coefficient  $(\hat{\mathbf{h}}_{i,s})_i$  individually. In addition, denoted as U-G-HBF-2GCN, an unrolled DN employing separate GCNs, and thus separate virtual channel covariances  $\hat{\Psi}_{i,j}$ , for the analog beams and digital precoders is evaluated. This mimics the slower reconfiguration capability of analog components, which therefore rely on the channel statistics, while the quickly configurable digital precoders leverage instantaneous information. The outage probability is evaluated w.r.t. instantaneous CSI.

Tab. 4 shows that the proposed architecture U-G-HBF-2GCN significantly outperforms the baseline G-HBF-marg for 2 users and all investigated values of  $N_{\text{fb}}$ , thereby clearly improving the allocated power if  $N_{\text{fb}}$  increases. The outage constraint for a single user is overfulfilled while the corresponding dual variables remain zero during training. This behavior may be caused by insufficient degrees of freedom in the GCN architecture or the channel mapping in (27). In comparison, U-G-HBF-GCN does not significantly outperform G-HBF-marg, demonstrating the benefit of separate GCNs for statistical and instantaneous CSI.

#### VI. Conclusion and Outlook

We propose a novel deep-learning-based model architecture for hybrid downlink beamforming under probabilistic QoS constraints. To compute the model gradient, we derive a computationally efficient gradient for the widely applicable constrained uplink/downlink beamforming problem and establish sufficient conditions for its existence. Experiments show that the proposed method can satisfy multiple outage constraints while outperforming the benchmarks in terms of total allocated power. In addition, the proposed methods exhibit an excellent capability of generalizing to different levels of imperfect channel state information and numbers of users, even when extrapolating to an unseen number of users. With a sufficient number of RF chains, hybrid beamforming attains performance comparable to a reduced deep network architecture designed for fully digital beamforming. We further demonstrate that an alternative annealing-based approach for enforcing probabilistic constraints reduces training time by smoothing the loss landscape, while also yielding slightly improved deep network performance.

**TABLE 3. Results for  $M = 4 \times 4$  antennas with 1 to 4 users for nominal outage  $P_{\text{out}} = 0.10$  for CSI degradation based on different  $P_{\text{pil},i}$ . U-G-HBF-GCN\* is trained with 2-3 users.**

$P_{\text{pil},i}$	Methods	1 user		2 users		3 users		4 users	
		$\ \mathbf{p}\ _1$	$\hat{P}_{\text{out}} [\%]$	$\ \mathbf{p}\ _1$	$\hat{P}_{\text{out}} [\%]$	$\ \mathbf{p}\ _1$	$\hat{P}_{\text{out}} [\%]$	$\ \mathbf{p}\ _1$	$\hat{P}_{\text{out}} [\%]$
10dB	G-HBF-perf	1.30 ± 0.05	0.00 ± 0.00	3.02 ± 0.08	0.00 ± 0.00	5.18 ± 0.11	0.00 ± 0.00	8.23 ± 0.21	0.00 ± 0.00
	G-HBF-marg	1.67 ± 0.06	10.05 ± 0.04	4.56 ± 0.13	10.02 ± 0.05	10.23 ± 0.26	10.04 ± 0.03	29.81 ± 1.78	10.01 ± 0.03
	U-G-HBF-GCN	1.34 ± 0.05	9.62 ± 1.09	3.70 ± 0.22	9.07 ± 1.15	7.66 ± 0.51	9.82 ± 0.67	16.23 ± 1.24	11.97 ± 0.90
	U-G-HBF-GCN*	1.31 ± 0.06	9.65 ± 1.44	3.53 ± 0.10	9.49 ± 0.63	7.72 ± 0.50	10.79 ± 0.45	17.35 ± 1.57	15.94 ± 1.23
	U-FDBF-GCN	1.26 ± 0.04	8.90 ± 0.82	3.32 ± 0.09	8.85 ± 0.62	6.38 ± 0.27	9.83 ± 0.60	11.73 ± 0.93	11.28 ± 1.29
24dB	G-HBF-perf	1.26 ± 0.06	0.00 ± 0.00	3.04 ± 0.10	0.00 ± 0.00	5.24 ± 0.03	0.00 ± 0.00	8.26 ± 0.19	0.00 ± 0.00
	G-HBF-marg	1.32 ± 0.06	10.05 ± 0.04	3.21 ± 0.10	10.02 ± 0.05	5.63 ± 0.03	10.01 ± 0.03	9.08 ± 0.21	9.98 ± 0.05
	U-G-HBF-GCN	1.04 ± 0.03	6.74 ± 0.91	2.43 ± 0.05	7.90 ± 0.74	4.19 ± 0.11	8.73 ± 0.36	6.82 ± 0.15	8.99 ± 0.79
	U-G-HBF-GCN*	1.01 ± 0.03	7.28 ± 0.65	2.39 ± 0.03	8.33 ± 0.88	4.15 ± 0.07	9.28 ± 0.36	6.82 ± 0.15	9.93 ± 0.75
	U-FDBF-GCN	0.98 ± 0.02	7.14 ± 0.81	2.20 ± 0.04	7.89 ± 0.91	3.61 ± 0.07	8.69 ± 0.30	5.41 ± 0.07	8.91 ± 0.43

**TABLE 4. Results for  $M = 8 \times 8$  antennas for combined statistical and instantaneous CSI with DFT feedback quantization.**

#users $I$	Methods	$N_{\text{fb}} \in \{4, \dots, 8\}$		$N_{\text{fb}} = 4$		$N_{\text{fb}} = 6$		$N_{\text{fb}} = 8$	
		$\ \mathbf{p}\ _1$	$\hat{P}_{\text{out}} [\%]$	$\ \mathbf{p}\ _1$	$\hat{P}_{\text{out}} [\%]$	$\ \mathbf{p}\ _1$	$\hat{P}_{\text{out}} [\%]$	$\ \mathbf{p}\ _1$	$\hat{P}_{\text{out}} [\%]$
1	G-HBF-perf	1.07 ± 0.04	0.00 ± 0.00	1.09 ± 0.03	0.00 ± 0.00	1.07 ± 0.03	0.00 ± 0.00	1.05 ± 0.02	0.00 ± 0.00
	G-HBF-marg	2.03 ± 0.05	10.01 ± 0.04	3.82 ± 0.27	10.00 ± 0.03	1.99 ± 0.10	10.00 ± 0.03	1.49 ± 0.06	9.97 ± 0.05
	U-G-HBF-GCN	2.30 ± 0.11	1.32 ± 0.89	4.33 ± 0.30	2.22 ± 0.37	2.22 ± 0.12	1.38 ± 1.22	1.61 ± 0.09	1.07 ± 0.72
	U-G-HBF-2GCN	1.05 ± 0.05	5.33 ± 0.29	1.22 ± 0.06	4.26 ± 0.58	1.05 ± 0.03	5.67 ± 0.45	0.95 ± 0.02	6.53 ± 0.91
2	G-HBF-perf	2.60 ± 0.09	0.00 ± 0.00	2.61 ± 0.11	0.04 ± 0.08	2.61 ± 0.08	0.00 ± 0.00	2.59 ± 0.08	0.01 ± 0.01
	G-HBF-marg	4.41 ± 0.35	10.02 ± 0.03	6.55 ± 0.36	10.00 ± 0.04	4.38 ± 0.19	10.01 ± 0.05	3.67 ± 0.16	10.01 ± 0.05
	U-G-HBF-GCN	4.35 ± 0.13	8.78 ± 0.79	6.30 ± 0.63	9.20 ± 1.73	4.22 ± 0.25	8.66 ± 0.68	3.43 ± 0.15	9.63 ± 1.30
	U-G-HBF-2GCN	3.15 ± 0.08	9.64 ± 0.68	3.95 ± 0.15	9.91 ± 1.00	3.09 ± 0.11	9.85 ± 1.09	2.66 ± 0.06	9.68 ± 0.81

Future work could explore virtual channel mappings with higher degrees of freedom, pruning techniques for the analog codebook, alternative hybrid architectures as well as multi-carrier and multi-cell systems. Furthermore, reinforcement learning could be investigated to eliminate the requirement for exact channel state information during training.

## Appendix A Jacobi Matrices of the Baseband BF Problem

In the following, the Jacobi matrices corresponding to the SNLE (45) for the digital BF problem are detailed. We adopt the notation of [81] that  $\text{vec}(\Psi) = \Gamma_{\text{d}} \hat{\psi}_{\text{d}} + \Gamma_{\text{re}} \hat{\psi}_{\text{re}} + \mathbf{j} \Gamma_{\text{im}} \hat{\psi}_{\text{im}}$ , where  $\hat{\psi}_{\text{d}} \in \mathbb{R}^{M_{\text{rf}}}$ ,  $\hat{\psi}_{\text{re}} \in \mathbb{R}^{M_{\text{rf}}(M_{\text{rf}}-1)/2}$  and  $\hat{\psi}_{\text{im}} \in \mathbb{R}^{M_{\text{rf}}(M_{\text{rf}}-1)/2}$  are the diagonal, real upper triangular and imaginary upper triangular of  $\hat{\Psi} \in \mathbb{R}^{M_{\text{rf}} \times M_{\text{rf}}}$ , respectively, and  $\Gamma_{\text{d}}$ ,  $\Gamma_{\text{re}}$  and  $\Gamma_{\text{im}}$  are the associated mapping matrices. Further, note that we can rewrite  $\mathbf{g}_{\text{b}}$  in (45) as

$$\mathbf{g}_{\text{b}}(\check{\zeta}, \hat{\psi}) = \left[ \left( \underline{\Lambda}_1(\mathbf{q}, \hat{\psi}) \check{\mathbf{b}}_1 \right)^{\text{T}} \cdots \left( \underline{\Lambda}_I(\mathbf{q}, \hat{\psi}) \check{\mathbf{b}}_I \right)^{\text{T}} \right]^{\text{T}} \quad (57)$$

where we define

$$\underline{\Lambda}_i(\mathbf{q}, \hat{\psi}) = \hat{\Psi}_{0,i} - \gamma_i^{-1} q_i \hat{\Psi}_{i,i} + \sum_{j \neq i} q_j \hat{\Psi}_{j,i} \quad (58)$$

$$\text{and } \hat{\Psi}_{i,j} = \begin{bmatrix} \Re(\hat{\Psi}_{i,j}) & -[\Im(\hat{\Psi}_{i,j})]_{:, -M_{\text{rf}}} \\ [\Im(\hat{\Psi}_{i,j})]_{-M_{\text{rf}}, :} & [\Re(\hat{\Psi}_{i,j})]_{-M_{\text{rf}}, -M_{\text{rf}}} \end{bmatrix}. \quad (59)$$

In the following, the arguments  $(\check{\zeta}, \hat{\psi})$  are omitted for readability.

### 1) Left-hand side

The left-hand side is decomposed as

$$\mathbf{D}_{\check{\zeta}} \mathbf{g} = \begin{bmatrix} \mathbf{D}_{\check{\zeta}} \mathbf{g}_{\text{b}} & \mathbf{D}_{\mathbf{q}} \mathbf{g}_{\text{q}} \\ \mathbf{D}_{\check{\zeta}} \mathbf{g}_{\text{q}} & \mathbf{D}_{\mathbf{q}} \mathbf{g}_{\text{q}} \end{bmatrix}. \quad (60)$$

For the upper left block, we have

$$\mathbf{D}_{\check{\zeta}} \mathbf{g}_{\text{b}} = \text{Blkdiag}(\mathbf{D}_{\check{\zeta}_1} \mathbf{g}_{\text{b},1}, \dots, \mathbf{D}_{\check{\zeta}_I} \mathbf{g}_{\text{b},I}), \quad (61)$$

$$\mathbf{D}_{\check{\zeta}_i} \mathbf{g}_{\text{b},i} = \underline{\Lambda}_i(\mathbf{q}, \hat{\psi}). \quad (62)$$

The upper left block is itself composed of sub-blocks

$$\mathbf{D}_{\mathbf{q}} \mathbf{g}_{\text{b}} = \begin{bmatrix} \mathbf{D}_{q_j} \mathbf{g}_{\text{b}_i} & \xrightarrow{j} \\ \downarrow i & \ddots \end{bmatrix}, \quad (63)$$

$$\text{where } \mathbf{D}_{q_j} \mathbf{g}_{\text{b},i} = \begin{cases} -\gamma_i^{-1} \hat{\Psi}_{i,i} \check{\mathbf{b}}_i & \text{for } j = i, \\ \hat{\Psi}_{j,i} \check{\mathbf{b}}_i & \text{for } j \neq i. \end{cases} \quad (64)$$

Leveraging symmetry, the lower left block is constructed as

$$\mathbf{D}_{\check{\zeta}} \mathbf{g}_{\text{q}} = 2 \text{Diag}(\mathbf{q}) \mathbf{D}_{\mathbf{q}} \mathbf{g}_{\text{b}}^{\text{T}}, \quad (65)$$

while for the lower right block, we have

$$\mathbf{D}_{\mathbf{q}} \mathbf{g}_{\text{q}} = \text{Diag}(\mathbf{D}_{q_1} \mathbf{g}_{\text{q},1}, \dots, \mathbf{D}_{q_I} \mathbf{g}_{\text{q},I}), \quad (66)$$

$$\text{with } \mathbf{D}_{q_i} \mathbf{g}_{\text{q},i} = 1 - \gamma_i^{-1} \check{\mathbf{b}}_i^{\text{T}} \hat{\Psi}_{i,i} \check{\mathbf{b}}_i + \sum_{j \neq i} \check{\mathbf{b}}_j^{\text{T}} \hat{\Psi}_{i,j} \check{\mathbf{b}}_j. \quad (67)$$

Note that if the problem is feasible, the SINR is exactly achieved [82], thus,  $D_q \underline{g}_q|_{\zeta=\zeta^*} = \mathbf{0}$ .

## 2) Right-hand side

Decompose the right-hand side as

$$D_{\hat{\psi}} \underline{g} = \begin{bmatrix} D_{\hat{\psi}_{i,j}} \underline{g}_b \\ D_{\hat{\psi}_{i,j}} \underline{g}_q \end{bmatrix}. \quad (68)$$

The upper block is constructed as

$$D_{\hat{\psi}_{i,j}} \underline{g}_b = \begin{bmatrix} k \downarrow & D_{\hat{\psi}_{d,(i,j)}} \underline{g}_{b,k} & D_{\hat{\psi}_{re,(i,j)}} \underline{g}_{b,k} & D_{\hat{\psi}_{im,(i,j)}} \underline{g}_{b,k} \end{bmatrix}, \quad (69)$$

where, for  $\alpha \in \{d, re\}$ , we have ( $\mathbf{I}$  has size  $M_{rf} \times M_{rf}$ )

$$D_{\hat{\psi}_{\alpha,(i,j)}} \underline{g}_{b,k} = \begin{cases} -\frac{q_i}{\gamma_i} \begin{bmatrix} \Re(\check{\mathbf{b}}_i^T \otimes \mathbf{I}) \Gamma_\alpha \\ [\Im(\check{\mathbf{b}}_i^T \otimes \mathbf{I})]_{:, -M_{rf}} \Gamma_\alpha \end{bmatrix} & \text{for } i = j = k, \\ q_i \begin{bmatrix} \Re(\check{\mathbf{b}}_i^T \otimes \mathbf{I}) \Gamma_\alpha \\ [\Im(\check{\mathbf{b}}_i^T \otimes \mathbf{I})]_{:, -M_{rf}} \Gamma_\alpha \end{bmatrix} & \text{for } i \neq 0, \\ & i \neq j, j = k, \\ \begin{bmatrix} \Re(\check{\mathbf{b}}_i^T \otimes \mathbf{I}) \Gamma_\alpha \\ [\Im(\check{\mathbf{b}}_i^T \otimes \mathbf{I})]_{:, -M_{rf}} \Gamma_\alpha \end{bmatrix} & \text{for } i = 0, \\ & i \neq j, j = k, \\ \mathbf{0} & \text{otherwise.} \end{cases} \quad (70)$$

For  $\alpha = im$ , we have

$$D_{\hat{\psi}_{im,(i,j)}} \underline{g}_{b,k} = \begin{cases} -\frac{q_i}{\gamma_i} \begin{bmatrix} (-\Im(\check{\mathbf{b}}_i^T \otimes \mathbf{I}) \Gamma_\alpha \\ [\Re(\check{\mathbf{b}}_i^T \otimes \mathbf{I})]_{:, -M_{rf}} \Gamma_\alpha \end{bmatrix} & \text{for } i = j = k, \\ q_i \begin{bmatrix} (-\Im(\check{\mathbf{b}}_i^T \otimes \mathbf{I}) \Gamma_\alpha \\ [\Re(\check{\mathbf{b}}_i^T \otimes \mathbf{I})]_{:, -M_{rf}} \Gamma_\alpha \end{bmatrix} & \text{for } i \neq 0, \\ & i \neq j, j = k, \\ \begin{bmatrix} (-\Im(\check{\mathbf{b}}_i^T \otimes \mathbf{I}) \Gamma_\alpha \\ [\Re(\check{\mathbf{b}}_i^T \otimes \mathbf{I})]_{:, -M_{rf}} \Gamma_\alpha \end{bmatrix} & \text{for } i = 0, \\ & j = k, \\ \mathbf{0} & \text{otherwise.} \end{cases} \quad (71)$$

For the lower block, we similarly have

$$D_{\hat{\psi}_{i,j}} \underline{g}_q = \begin{bmatrix} k \downarrow & D_{\hat{\psi}_{d,(i,j)}} \underline{g}_{q,k} & D_{\hat{\psi}_{re,(i,j)}} \underline{g}_{q,k} & D_{\hat{\psi}_{im,(i,j)}} \underline{g}_{q,k} \end{bmatrix}, \quad (72)$$

where for  $\alpha \in \{d, re\}$

$$D_{\hat{\psi}_{\alpha,(i,j)}} \underline{g}_{q,k} = \begin{cases} -\frac{q_i}{\gamma_i} \Re(\text{vec}(\check{\mathbf{b}}_i \check{\mathbf{b}}_i^H)) \Gamma_\alpha & \text{for } i = j = k \\ q_i \Re(\text{vec}(\check{\mathbf{b}}_j \check{\mathbf{b}}_j^H)) \Gamma_\alpha & \text{for } i = k, i \neq j \\ 0 & \text{otherwise.} \end{cases} \quad (73)$$

Lastly, for  $\alpha = im$ , we have

$$D_{\hat{\psi}_{im,(i,j)}} \underline{g}_{q,k} = \begin{cases} -\frac{q_i}{\gamma_i} \Im(\text{vec}(\check{\mathbf{b}}_i \check{\mathbf{b}}_i^H)) \Gamma_\alpha & \text{for } i = j = k \\ q_i \Im(\text{vec}(\check{\mathbf{b}}_j \check{\mathbf{b}}_j^H)) \Gamma_\alpha & \text{for } i = k, i \neq j \\ 0 & \text{otherwise.} \end{cases} \quad (74)$$

## 3) Beamformer normalization

The associated Jacobi matrix with the beamformer normalization can be found as

$$D_{\check{\zeta}} \mathbf{f}_{BN}(\check{\zeta}) = \text{Blkdiag} \left( D_{\check{\mathbf{b}}_1} \check{\mathbf{f}}_{BN}(\check{\mathbf{b}}_1), \dots, D_{\check{\mathbf{b}}_I} \check{\mathbf{f}}_{BN}(\check{\mathbf{b}}_I), \mathbf{I}_{I \times I} \right), \quad (75)$$

$$D_{\check{\mathbf{b}}_i} \check{\mathbf{f}}_{BN}(\check{\mathbf{b}}_i) = \frac{1}{\|\check{\mathbf{b}}_i\|_2^{\frac{3}{2}}} \left( \|\check{\mathbf{b}}_i\|_2^2 \mathbf{I} - \begin{bmatrix} \Re(\check{\mathbf{b}}_i) \Re(\check{\mathbf{b}}_i)^T & \Re(\check{\mathbf{b}}_i) [\Im(\check{\mathbf{b}}_i)]_{-M_{rf}}^T \\ \Im(\check{\mathbf{b}}_i) \Re(\check{\mathbf{b}}_i)^T & \Im(\check{\mathbf{b}}_i) [\Im(\check{\mathbf{b}}_i)]_{-M_{rf}}^T \end{bmatrix} \right). \quad (76)$$

## Appendix B

### Identification of the Derivative

*Proof of Theorem IV.2:*

We first argue that a solution of Problem (31) with  $[\Im(\check{\mathbf{b}}_i^*)]_{M_{rf}} = 0$  for all  $i$  corresponds to a critical point of  $\underline{g}(\check{\zeta}, \hat{\psi})$ . The semidefinite relaxation of the dual downlink problem corresponding to Problem (31) to the convex formulation in (38) is exact, c.f. [69], [70, Th. 3.2]. Since KKT conditions are necessary and sufficient in this case [65, Ch. 5.5.3], it follows from Lemma IV.1 that any solution  $(\mathbf{b}_i^*, q_i^*)_i$  of Problem (31) has a corresponding dual feasible solution  $(\check{\mathbf{b}}_i^*, q_i^*)_i = (\sqrt{p_i^*} \mathbf{b}_i^*, q_i^*)_i$  to the SNLE (42)-(43), where the downlink power  $(p_i^*)_i$  is given by (32). Due to arbitrariness of the baseband beamformers' phase rotations, we can assume without loss of generality that  $[\Im(\check{\mathbf{b}}_i^*)]_{M_{rf}} = 0$  for all  $i$ . We thus conclude from the definition of  $\underline{g}(\check{\zeta}, \hat{\psi})$  in (45) that  $\underline{g}(\check{\zeta}^*, \hat{\psi}) = \mathbf{0}$ , where  $\check{\zeta}^*$  is defined analogously to (44).

We now show by contradiction that  $D_{\check{\zeta}} \underline{g}(\check{\zeta}^*, \hat{\psi})$  is not rank-deficient. Suppose  $D_{\check{\zeta}} \underline{g}(\check{\zeta}^*, \hat{\psi})$  is rank-deficient, then  $D_{\check{\zeta}} \underline{g}(\check{\zeta}^*, \hat{\psi}) \check{\zeta}' = \mathbf{0}$  for some  $\check{\zeta}' = [(\check{\mathbf{b}}')^T (q')^T]^T \neq \mathbf{0}$ . Leveraging the symmetry in (65), this can be written as (the argument  $\hat{\psi}$  is omitted for readability)

$$D_{\check{\mathbf{b}}} \underline{g}_b(\check{\zeta}^*) \check{\mathbf{b}}' + \frac{1}{2} D_{\mathbf{b}} \underline{g}_q^T(\check{\zeta}^*) \text{Diag}(q^*)^{-1} q' = \mathbf{0}, \quad (77)$$

$$D_{\check{\mathbf{b}}} \underline{g}_q(\check{\zeta}^*) \check{\mathbf{b}}' = \mathbf{0}. \quad (78)$$

First, consider the case  $\check{\mathbf{b}}' \neq \mathbf{0}$ . Multiplying  $(\check{\mathbf{b}}')^T$  from the left to (77) and  $(q')^T \text{Diag}(q^*)^{-1}$  to (78) yields

$$(\check{\mathbf{b}}')^T D_{\check{\mathbf{b}}} \underline{g}_b(\check{\zeta}^*) \check{\mathbf{b}}' + \frac{1}{2} \check{\mathbf{b}}'^T D_q \underline{g}_q^T(\check{\zeta}^*) \text{Diag}(q^*)^{-1} q' = 0, \quad (79)$$

$$(q')^T \text{Diag}(q^*)^{-1} D_{\check{\mathbf{b}}} \underline{g}_q(\check{\zeta}^*) \check{\mathbf{b}}' = 0, \quad (80)$$

and thus  $(\check{\mathbf{b}}')^T D_{\check{\mathbf{b}}} \underline{g}_b(\check{\zeta}^*) \check{\mathbf{b}}' = 0$  by substituting (80) into (79). Since  $\underline{\Lambda}_i(q^*) \succeq \mathbf{0}$  (dual feasible solution), we know that  $\underline{\Lambda}_i(q^*) \succeq \mathbf{0}$  and that  $D_{\check{\mathbf{b}}} \underline{g}_b(\check{\zeta}^*) \succeq \mathbf{0}$  as well. Therefore, we deduce that  $\check{\mathbf{b}}' \in \ker(D_{\check{\mathbf{b}}} \underline{g}_b(\check{\zeta}^*))$ , where  $\ker(\cdot)$  denotes the matrix kernel.

Let us now rewrite  $\check{\mathbf{b}}_i^*$  as  $\check{\mathbf{b}}_i^* = s_i^* \mathbf{b}_i^*$  with normalized real-valued baseband beamformers  $\|\mathbf{b}_i^*\|_2 = 1$  and scale  $s_i^* > 0$

for all  $i = 1, \dots, I$ . Further define  $\widehat{\mathbf{C}}((\mathbf{x}_i)_i, (\mathbf{y}_i)_i) \in \mathbb{R}^{I \times I}$  as

$$[\widehat{\mathbf{C}}((\mathbf{x}_i)_i, (\mathbf{y}_i)_i)]_{j,k} = \begin{cases} \gamma_j^{-1} \mathbf{x}_j^T \widehat{\Psi}_{j,j} \mathbf{y}_j & \text{for } j = k, \\ -\mathbf{x}_k^T \widehat{\Psi}_{j,k} \mathbf{y}_k & \text{for } j \neq k, \end{cases} \quad (81)$$

where  $(\mathbf{x}_i)_i$  and  $(\mathbf{y}_i)_i$  are conformable arguments. Suppose that  $\check{\mathbf{b}}'_i = \pm s'_i \mathbf{b}_i^*$  for some  $s'_i > 0$  for all  $i$ , which immediately implies  $\check{\mathbf{b}}' \in \ker(\mathbf{D}_{\check{\mathbf{b}}} \mathbf{g}_{\check{\mathbf{b}}}(\check{\boldsymbol{\zeta}}^*))$ . Additionally, rewrite the left-hand side of (78) as

$$\mathbf{D}_{\check{\mathbf{b}}} \mathbf{g}_{\check{\mathbf{q}}}(\check{\boldsymbol{\zeta}}^*) \check{\mathbf{b}}' = -2 \text{Diag}(\mathbf{q}^*) \widehat{\mathbf{C}}((\mathbf{b}_i^*)_i, (\mathbf{b}_i^*)_i) (\mathbf{s}^* \odot \mathbf{s}'). \quad (82)$$

We can identify the coupling matrix  $\widehat{\mathbf{C}}((\mathbf{b}_i^*)_i, (\mathbf{b}_i^*)_i) = \widehat{\mathbf{C}}_C(\mathbf{B}^*, \mathbf{A})$  (see definition in (33)), which has full rank since  $\mathbf{B}^*$  is a solution to the baseband optimization problem [82]. It follows that (82) can only be  $\mathbf{0}$  if  $\mathbf{s}' = \mathbf{0}$ .

Therefore, suppose instead  $\check{\mathbf{b}}'_i = s'_i \mathbf{b}'_i$ , where  $\mathbf{b}'_i \neq \pm \mathbf{b}_i^*$  for some  $i = k$ . Since we require that  $\check{\mathbf{b}}' \in \ker(\mathbf{D}_{\check{\mathbf{b}}} \mathbf{g}_{\check{\mathbf{b}}}(\check{\boldsymbol{\zeta}}^*))$ , it is implied that  $\dim \ker(\underline{\mathbf{A}}_k(\mathbf{q}^*)) \geq 2$ . As such, there also exists a  $\check{\boldsymbol{\zeta}}''$  with  $\mathbf{b}''_k \neq \mathbf{b}_k^*$  and  $\mathbf{q}'' = \mathbf{q}^*$  such that  $\underline{\mathbf{A}}_k(\mathbf{q}^*) \mathbf{b}''_k$  and thus  $\mathbf{g}_{\check{\mathbf{b}}}(\check{\boldsymbol{\zeta}}'') = \mathbf{0}$ . The complementarity condition  $\mathbf{g}_{\check{\mathbf{q}}}(\check{\boldsymbol{\zeta}}'')$  can be expressed as

$$\mathbf{g}_{\check{\mathbf{q}}}(\check{\boldsymbol{\zeta}}'') = \text{Diag}(\mathbf{q}^*) \left( \mathbf{1} - \widehat{\mathbf{C}}((\mathbf{b}'_i)_i, (\mathbf{b}'_i)_i) (\mathbf{s}'' \odot \mathbf{s}'') \right). \quad (83)$$

Due to the lower semi-continuity of the rank, if  $\check{\boldsymbol{\zeta}}''$  is chosen sufficiently close to  $\check{\boldsymbol{\zeta}}^*$ , then  $\widehat{\mathbf{C}}((\mathbf{b}'_i)_i, (\mathbf{b}'_i)_i)$  still has rank  $I$ . Thus, we can find  $\mathbf{s}'' > \mathbf{0}$  such that  $\mathbf{g}_{\check{\mathbf{q}}}(\check{\boldsymbol{\zeta}}'') = \mathbf{0}$  holds and  $\check{\boldsymbol{\zeta}}''$  is a distinct primal and dual feasible critical point. In other words,  $\check{\boldsymbol{\zeta}}''$  constructs a distinct solution  $(\check{\mathbf{B}}''_i, q''_i)_i$  of Problem (38) different from  $(\check{\mathbf{B}}^*_i, q^*_i)_i = (\mathbf{b}_i \mathbf{b}_i^H, q^*_i)_i$ . Since this violates Assumption IV.1, we conclude that  $\check{\mathbf{b}} = \mathbf{0}$ .

Consider now  $\mathbf{q}'$ . As  $\check{\mathbf{b}}' = \mathbf{0}$ , we have  $\mathbf{D}_{\check{\mathbf{q}}} \mathbf{g}_{\check{\mathbf{b}}}(\check{\boldsymbol{\zeta}}^*) \mathbf{q}' = \mathbf{0}$ . After left-multiplying  $\text{Blkdiag}(\check{\mathbf{b}}_1^*, \dots, \check{\mathbf{b}}_I^*)^T$  on both sides, the following identity can be verified:

$$\begin{aligned} \mathbf{0} &= \text{Blkdiag}(\check{\mathbf{b}}_1^*, \dots, \check{\mathbf{b}}_I^*) \mathbf{D}_{\check{\mathbf{q}}} \mathbf{g}_{\check{\mathbf{b}}}(\check{\boldsymbol{\zeta}}^*) \mathbf{q}' \\ &= -\text{Diag}(\mathbf{s}^* \odot \mathbf{s}^*) \widehat{\mathbf{C}}^T((\mathbf{b}_i^*)_i, (\mathbf{b}_i^*)_i) \mathbf{q}'. \end{aligned} \quad (84)$$

Since both leading matrices in the second line of (84) have full rank, we conclude that  $\mathbf{q}' = \mathbf{0}$ . Therefore,  $\check{\boldsymbol{\zeta}}' = \mathbf{0}$  is the only solution to  $\mathbf{D}_{\check{\boldsymbol{\zeta}}} \mathbf{g}(\check{\boldsymbol{\zeta}}^*, \boldsymbol{\psi}) \check{\boldsymbol{\zeta}}' = \mathbf{0}$  and  $\mathbf{D}_{\check{\boldsymbol{\zeta}}} \mathbf{g}(\check{\boldsymbol{\zeta}}^*, \boldsymbol{\psi})$  has full rank.

As  $\check{\boldsymbol{\zeta}}^*$  constructs a solution of Problem (31) with  $[\mathfrak{S}(\check{\mathbf{b}}_i^*)]_{M_{\text{rf}}} = 0$  and is a critical point of  $\mathbf{g}(\check{\boldsymbol{\zeta}}^*, \boldsymbol{\psi})$ , and additionally  $\mathbf{D}_{\check{\boldsymbol{\zeta}}} \mathbf{g}(\check{\boldsymbol{\zeta}}^*, \boldsymbol{\psi})$  is nonsingular, the implicit function theorem [66, Th. 8.2] is applicable. Application of the chain rule due to the composition with the normalization in (48) immediately yields (49). ■

**Remark.** The nonsingularity of  $\mathbf{D}_{\check{\boldsymbol{\zeta}}} \mathbf{g}(\check{\boldsymbol{\zeta}}^*, \boldsymbol{\psi})$  implies that  $\check{\boldsymbol{\zeta}}^*$  is an *isolated* critical point of  $\mathbf{g}(\check{\boldsymbol{\zeta}}^*, \boldsymbol{\psi})$  [66, Corollary 7.8]. The equations that have been removed in (45) are indeed redundant.

## Appendix C Pseudocode of the Training Procedure

### Algorithm 1

---

```

input  $\mathcal{D}_{\text{train}}, \mathcal{D}_{\text{val}}, \boldsymbol{\theta}^{(0)}, \eta_{\text{p}}, \eta_{\text{d}}, \eta_{\text{a}}, \bar{\beta}_{\text{c}}, \eta_{\text{c}}, \tau_{\text{pat},1}, \tau_{\text{pat},2}, \tau_{\text{val}}, \bar{\lambda}_{\text{d}}$ 
 $\tau, \kappa \leftarrow 0, \boldsymbol{\lambda}^{(0)} \leftarrow \mathbf{0}$ 
 $\kappa_{\text{pat},1} \leftarrow \tau_{\text{pat},1} // \tau_{\text{val}}, \kappa_{\text{pat},2} \leftarrow \tau_{\text{pat},2} // \tau_{\text{val}}$ 
while True do
  if  $\tau \bmod \tau_{\text{val}} = 0$  then
     $J_{\text{cm}}^{(\kappa)} \leftarrow (55)$  with  $\bar{\lambda}_{\text{d}}$ 
    if  $\min_{\kappa'=0}^{\kappa} \{J_{\text{cm}}^{(\kappa')}\} < \min_{\kappa'=\max\{0, \kappa - \kappa_{\text{pat},1}\}}^{\kappa} \{J_{\text{cm}}^{(\kappa')}\}$  then
       $\eta_{\text{p}} \leftarrow \eta_{\text{a}} \eta_{\text{p}}, \eta_{\text{d}} \leftarrow \eta_{\text{a}} \eta_{\text{d}}$ 
       $\eta_{\text{a}} \leftarrow 1$ 
    if  $\min_{\kappa'=0}^{\kappa} \{J_{\text{cm}}^{(\kappa')}\} < \min_{\kappa'=\max\{0, \kappa - \kappa_{\text{pat},2}\}}^{\kappa} \{J_{\text{cm}}^{(\kappa')}\}$  then
      break
     $\kappa \leftarrow \kappa + 1$ 
  Sample minibatch  $\check{\mathcal{D}} \sim \mathcal{D}_{\text{train}}$ 
   $\boldsymbol{\theta}^{(\tau+1)} \leftarrow \boldsymbol{\theta}^{(\tau)} - \eta_{\text{p}} \text{AdamW}(\nabla_{\boldsymbol{\theta}} J(\check{\mathcal{D}}, \boldsymbol{\theta}^{(\tau)}, \boldsymbol{\lambda}^{(\tau)}), \boldsymbol{\theta}^{(\tau)})$  [74]
    with adaptive gradient clipping [75].
   $\boldsymbol{\lambda}^{(\tau+1)} \leftarrow [\boldsymbol{\lambda}^{(\tau)} + \eta_{\text{d}} \nabla_{\boldsymbol{\lambda}} J(\check{\mathcal{D}}, \boldsymbol{\theta}^{(\tau)}, \boldsymbol{\lambda}^{(\tau)})]_{\mathbf{0}}^{\infty}$ 
   $\beta_{\check{\boldsymbol{\zeta}}}^{(\tau+1)} \leftarrow (53)$  using  $\check{\mathcal{D}}$  with  $\bar{\beta}_{\text{c}}, \eta_{\text{c}}$ 
   $\tau \leftarrow \tau + 1$ 
return  $\boldsymbol{\theta}^{(\tau)}$ 

```

---

## REFERENCES

- [1] R. W. Heath Jr and A. Lozano, *Foundations of MIMO Communication*, 1st ed. Cambridge University Press, 2018.
- [2] X. You, C.-X. Wang, J. Huang, X. Gao, Z. Zhang, M. Wang, Y. Huang, C. Zhang, Y. Jiang, J. Wang, M. Zhu, B. Sheng, D. Wang, Z. Pan, P. Zhu, Y. Yang, Z. Liu, P. Zhang, X. Tao, S. Li, Z. Chen, X. Ma, C.-L. I, S. Han, K. Li, C. Pan, Z. Zheng, L. Hanzo, X. S. Shen, Y. J. Guo, Z. Ding, H. Haas, W. Tong, P. Zhu, G. Yang, J. Wang, E. G. Larsson, H. Q. Ngo, W. Hong, H. Wang, D. Hou, J. Chen, Z. Chen, Z. Hao, G. Y. Li, R. Tafazolli, Y. Gao, H. V. Poor, G. P. Fettweis, and Y.-C. Liang, "Towards 6G wireless communication networks: Vision, enabling technologies, and new paradigm shifts," *Science China Information Sciences*, vol. 64, no. 1, p. 110301, 2021.
- [3] C.-L. I, S. Han, and S. Bian, "Energy-Efficient 5G for a Greener Future," *Nature Electronics*, vol. 3, no. 4, pp. 182–184, 2020.
- [4] X. Cheng, Y. Hu, and L. Varga, "5G Network Deployment and the Associated Energy Consumption in the UK: A Complex Systems' Exploration," *Technological Forecasting and Social Change*, vol. 180, p. 121672, 2022.
- [5] W. Jiang, B. Han, M. A. Habibi, and H. D. Schotten, "The Road Towards 6G: A Comprehensive Survey," *IEEE Open Journal of the Communications Society*, vol. 2, pp. 334–366, 2021.
- [6] A. F. Molisch, V. V. Ratnam, S. Han, Z. Li, S. L. H. Nguyen, L. Li, and K. Haneda, "Hybrid Beamforming for Massive MIMO: A Survey," *IEEE Communications Magazine*, vol. 55, no. 9, pp. 134–141, 2017.
- [7] F. Sohrabi and W. Yu, "Hybrid Digital and Analog Beamforming Design for Large-Scale Antenna Arrays," *IEEE Journal of Selected Topics in Signal Processing*, vol. 10, no. 3, pp. 501–513, 2016.
- [8] N. Shlezinger, M. Ma, O. Lavi, N. T. Nguyen, Y. C. Eldar, and M. Juntti, "Artificial Intelligence-Empowered Hybrid Multiple-input/multiple-output Beamforming: Learning to Optimize for High-Throughput Scalable MIMO," *IEEE Vehicular Technology Magazine*, vol. 19, no. 3, pp. 58–67, 2024.
- [9] H. Joudeh and B. Clerckx, "Robust Transmission in Downlink Multiuser MISO Systems: A Rate-Splitting Approach," *IEEE Transactions on Signal Processing*, vol. 64, no. 23, pp. 6227–6242, 2016.
- [10] E. Bjornson, M. Bengtsson, and B. Ottersten, "Optimal Multiuser Transmit Beamforming: A Difficult Problem with a Simple Solution Structure [Lecture Notes]," *IEEE Signal Processing Magazine*, vol. 31, no. 4, pp. 142–148, 2014.

- [11] D. H. Nguyen and T. Le-Ngoc, "MMSE Precoding for Multiuser MISO Downlink Transmission with Non-Homogeneous User SNR Conditions," *EURASIP Journal on Advances in Signal Processing*, vol. 2014, no. 1, p. 85, 2014.
- [12] E. Bjornson, L. Sanguinetti, and M. Debbah, "Massive MIMO with Imperfect Channel Covariance Information," in *2016 50th Asilomar Conference on Signals, Systems and Computers*. Pacific Grove, CA, USA: IEEE, 2016, pp. 974–978.
- [13] K.-Y. Wang, A. M.-C. So, T.-H. Chang, W.-K. Ma, and C.-Y. Chi, "Outage Constrained Robust Transmit Optimization for Multiuser MISO Downlinks: Tractable Approximations by Conic Optimization," *IEEE Transactions on Signal Processing*, vol. 62, no. 21, pp. 5690–5705, 2014.
- [14] M. Botros Shenouda and T. N. Davidson, "Probabilistically-Constrained Approaches to the Design of the Multiple Antenna Downlink," in *2008 42nd Asilomar Conference on Signals, Systems and Computers*. Pacific Grove, CA, USA: IEEE, 2008, pp. 1120–1124.
- [15] I. Wajid, M. Pesavento, Y. C. Eldar, and D. Ciochina, "Robust Downlink Beamforming With Partial Channel State Information for Conventional and Cognitive Radio Networks," *IEEE Transactions on Signal Processing*, vol. 61, no. 14, pp. 3656–3670, 2013.
- [16] Y. Xu, X. Zhao, and Y.-C. Liang, "Robust Power Control and Beamforming in Cognitive Radio Networks: A Survey," *IEEE Communications Surveys & Tutorials*, vol. 17, no. 4, pp. 1834–1857, 2015.
- [17] N. Vucic and H. Boche, "Robust QoS-Constrained Optimization of Downlink Multiuser MISO Systems," *IEEE Transactions on Signal Processing*, vol. 57, no. 2, pp. 714–725, 2009.
- [18] C. Zhang, P. Patras, and H. Haddadi, "Deep Learning in Mobile and Wireless Networking: A Survey," *IEEE Communications Surveys & Tutorials*, vol. 21, no. 3, pp. 2224–2287, 2019.
- [19] R. Shafin, L. Liu, V. Chandrasekhar, H. Chen, J. Reed, and J. C. Zhang, "Artificial Intelligence-Enabled Cellular Networks: A Critical Path to Beyond-5G and 6G," *IEEE Wireless Communications*, vol. 27, no. 2, pp. 212–217, 2020.
- [20] K. Gregor and Y. LeCun, "Learning Fast Approximations of Sparse Coding," in *Proceedings of the 27th International Conference on International Conference on Machine Learning*, ser. ICML'10, 2010, pp. 399–406.
- [21] N. Shlezinger, Y. C. Eldar, and S. P. Boyd, "Model-Based Deep Learning: On the Intersection of Deep Learning and Optimization," *IEEE Access*, vol. 10, pp. 115 384–115 398, 2022.
- [22] L. Schynol and M. Pesavento, "Coordinated Sum-Rate Maximization in Multicell MU-MIMO with Deep Unrolling," *IEEE Journal on Selected Areas in Communications*, vol. 41, pp. 1120–1134, 2023.
- [23] Z. Wang, M. Li, Q. Liu, and A. L. Swindlehurst, "Hybrid Precoder and Combiner Design With Low-Resolution Phase Shifters in mmWave MIMO Systems," *IEEE Journal of Selected Topics in Signal Processing*, vol. 12, no. 2, pp. 256–269, 2018.
- [24] O. E. Ayach, S. Rajagopal, S. Abu-Surra, Z. Pi, and R. W. Heath, "Spatially Sparse Precoding in Millimeter Wave MIMO Systems," *IEEE Transactions on Wireless Communications*, vol. 13, no. 3, pp. 1499–1513, 2014.
- [25] A. Alkhateeb, O. El Ayach, G. Leus, and R. W. Heath, "Channel Estimation and Hybrid Precoding for Millimeter Wave Cellular Systems," *IEEE Journal of Selected Topics in Signal Processing*, vol. 8, no. 5, pp. 831–846, 2014.
- [26] A. M. Elbir, K. V. Mishra, S. A. Vorobyov, and R. W. Heath, "Twenty-Five Years of Advances in Beamforming: From Convex and Nonconvex Optimization to Learning Techniques," *IEEE Signal Processing Magazine*, vol. 40, no. 4, pp. 118–131, 2023.
- [27] S. Malla and G. Abreu, "Transmission Strategies in Multi-User Millimeter Wave Systems," in *2017 International Symposium on Wireless Communication Systems (ISWCS)*. Bologna: IEEE, 2017, pp. 54–59.
- [28] M. Tajallifar, A. R. Sharafat, and H. Yanikomeroglu, "QoS-Aware Hybrid Beamforming With Minimal Power in mmWave Massive MIMO Systems," *IEEE Access*, vol. 9, pp. 164 668–164 680, 2021.
- [29] B.-Y. Chen, Y.-F. Chen, and S.-M. Tseng, "Hybrid Beamforming and Data Stream Allocation Algorithms for Power Minimization in Multi-User Massive MIMO-OFDM Systems," *IEEE Access*, vol. 10, pp. 101 898–101 912, 2022.
- [30] S. H. Kim and H. Jin, "Hybrid Beamforming Based SWIPT System Satisfying Individual Rate and Energy Constraints," *IEEE Access*, vol. 12, pp. 5617–5629, 2024.
- [31] M. A. Vazquez, L. Blanco, and A. Perez-Neira, "Multiuser Downlink Hybrid Analog-Digital Beamforming with Individual SINR Constraints," in *WSA 2017; 21th International ITG Workshop on Smart Antennas*, 2017, pp. 1–6.
- [32] G. Zang, L. Hu, F. Yang, L. Ding, and H. Liu, "Partially-Connected Hybrid Beamforming for Multi-User Massive MIMO Systems," *IEEE Access*, vol. 8, pp. 215 287–215 298, 2020.
- [33] L. Wen, H. Qian, M. Li, X. Luo, and K. Kang, "QoS-Guaranteed Hybrid Beamforming Design for Multi-User Systems With Finite-Resolution Phase Shifters," *IEEE Transactions on Green Communications and Networking*, vol. 7, no. 4, pp. 1678–1691, 2023.
- [34] R. Ye, S. He, Y. Huang, B. Jiang, and M. Su, "Power Minimization Hybrid Precoding for Millimeter Wave Communication Systems," in *2016 IEEE International Conference on Communication Systems (ICCS)*. Shenzhen, China: IEEE, 2016, pp. 1–6.
- [35] G. Hegde, Y. Cheng, and M. Pesavento, "Hybrid Beamforming for Large-Scale MIMO Systems Using Uplink-Downlink Duality," in *2017 IEEE International Conference on Acoustics, Speech and Signal Processing (ICASSP)*. New Orleans, LA: IEEE, 2017, pp. 3484–3488.
- [36] M. Tajallifar, A. R. Sharafat, and H. Yanikomeroglu, "Robust and Feasible QoS-Aware mmWave Massive MIMO Hybrid Beamforming," *IEEE Transactions on Wireless Communications*, vol. 23, no. 2, pp. 1520–1534, 2024.
- [37] Q. Hu, Y. Cai, Q. Shi, K. Xu, G. Yu, and Z. Ding, "Iterative Algorithm Induced Deep-Unfolding Neural Networks: Precoding Design for Multiuser MIMO Systems," *IEEE Transactions on Wireless Communications*, vol. 20, no. 2, pp. 1394–1410, 2021.
- [38] W. Jin, J. Zhang, C.-K. Wen, and S. Jin, "Model-Driven Deep Learning for Hybrid Precoding in Millimeter Wave MU-MIMO System," *IEEE Transactions on Communications*, vol. 71, no. 10, pp. 5862–5876, 2023.
- [39] W. Jin, J. Zhang, C.-K. Wen, S. Jin, X. Li, and S. Han, "Low-Complexity Joint Beamforming for RIS-Assisted MU-MISO Systems Based on Model-Driven Deep Learning," *IEEE Transactions on Wireless Communications*, vol. 23, no. 7, pp. 6968–6982, 2024.
- [40] Y. Liu, Y. Wang, J. Wang, L. You, W. Wang, and X. Gao, "Robust Downlink Precoding for LEO Satellite Systems With Per-Antenna Power Constraints," *IEEE Transactions on Vehicular Technology*, vol. 71, no. 10, pp. 10 694–10 711, 2022.
- [41] J. Shi, W. Wang, X. Yi, X. Gao, and G. Y. Li, "Deep Learning-Based Robust Precoding for Massive MIMO," *IEEE Transactions on Communications*, vol. 69, no. 11, pp. 7429–7443, 2021.
- [42] W. Xia, G. Zheng, Y. Zhu, J. Zhang, J. Wang, and A. P. Petropulu, "A Deep Learning Framework for Optimization of MISO Downlink Beamforming," *IEEE Transactions on Communications*, vol. 68, no. 3, pp. 1866–1880, 2020.
- [43] O. Lavi and N. Shlezinger, "Learn to Rapidly and Robustly Optimize Hybrid Precoding," *IEEE Transactions on Communications*, vol. 71, no. 10, pp. 5814–5830, 2023.
- [44] L. Wang, S. A. Vorobyov, and E. Ollila, "Robust Hybrid Beamforming for Integrated Sensing and Communications via Learned Optimization," in *ICASSP 2025 - 2025 IEEE International Conference on Acoustics, Speech and Signal Processing (ICASSP)*. Hyderabad, India: IEEE, 2025, pp. 1–5.
- [45] W. Liu, H. Xu, X. He, Y. Ye, and A. Zhou, "Bi-Level Deep Unfolding Based Robust Beamforming Design for IRS-Assisted ISAC System," *IEEE Access*, vol. 12, pp. 76 663–76 672, 2024.
- [46] S. Shrestha, X. Fu, and M. Hong, "Optimal Solutions for Joint Beamforming and Antenna Selection: From Branch and Bound to Graph Neural Imitation Learning," *IEEE Transactions on Signal Processing*, vol. 71, pp. 831–846, 2023.
- [47] C. Psomas, M. You, K. Liang, G. Zheng, and I. Krikidis, "Design and Analysis of SWIPT With Safety Constraints," *Proceedings of the IEEE*, vol. 110, no. 1, pp. 107–126, 2022.
- [48] M. Ying, X. Chen, Q. Qi, and W. Gerstaecker, "Deep Learning-Based Joint Channel Prediction and Multibeam Precoding for LEO Satellite Internet of Things," *IEEE Transactions on Wireless Communications*, vol. 23, no. 10, pp. 13 946–13 960, 2024.
- [49] H. S. Jang, H. Lee, and T. Q. S. Quek, "Deep Learning Approach for Outage-Constrained Non-Orthogonal Random Access," *IEEE Wireless Communications Letters*, vol. 11, no. 3, pp. 645–649, 2022.
- [50] M. You, G. Zheng, and H. Sun, "A Data Augmentation based DNN Approach for Outage-Constrained Robust Beamforming," in *2021*

- IEEE International Conference on Communications (ICC)*. Montreal, QC, Canada: IEEE, 2021, pp. 1–5.
- [51] K. Liang, G. Zheng, Z. Li, K.-K. Wong, and C.-B. Chae, “A Data and Model-Driven Deep Learning Approach to Robust Downlink Beamforming Optimization,” *IEEE Journal on Selected Areas in Communications*, vol. 42, no. 11, pp. 3278–3292, 2024.
- [52] S. He, J. Wang, Y. Huang, B. Ottersten, and W. Hong, “Codebook-Based Hybrid Precoding for Millimeter Wave Multiuser Systems,” *IEEE Transactions on Signal Processing*, vol. 65, no. 20, pp. 5289–5304, 2017.
- [53] L. Schynol, M. Hemsing, and M. Pesavento, “Codebook-Based Downlink Beamforming with Imperfect CSI Using Model-Driven Deep Learning,” in *2024 58th Asilomar Conference on Signals, Systems, and Computers*. Pacific Grove, CA, USA: IEEE, 2024, pp. 583–590.
- [54] M. Shao and W.-K. Ma, “A Simple Way to Approximate Average Robust Multiuser MISO Transmit Optimization Under Covariance-Based CSIT,” in *2017 IEEE International Conference on Acoustics, Speech and Signal Processing (ICASSP)*. New Orleans, LA: IEEE, 2017, pp. 3504–3508.
- [55] M. Eisen and A. Ribeiro, “Optimal Wireless Resource Allocation With Random Edge Graph Neural Networks,” *IEEE Transactions on Signal Processing*, vol. 68, pp. 2977–2991, 2020.
- [56] B. Song, R. L. Cruz, and B. D. Rao, “Network Duality for Multiuser MIMO Beamforming Networks and Applications,” *IEEE Transactions on Communications*, vol. 55, no. 3, pp. 618–630, 2007.
- [57] F. Rashid-Farrokhi, L. Tassiulas, and K. R. Liu, “Joint Optimal Power Control and Beamforming in Wireless Networks Using Antenna Arrays,” *IEEE Transactions on Communications*, vol. 46, no. 10, pp. 1313–1324, 1998.
- [58] M. Schubert and H. Boche, “Solution of the Multiuser Downlink Beamforming Problem With Individual SINR Constraints,” *IEEE Transactions on Vehicular Technology*, vol. 53, no. 1, pp. 18–28, 2004.
- [59] T. N. Kipf and M. Welling, “Semi-Supervised Classification with Graph Convolutional Networks,” in *Proceedings of the 5th International Conference on Learning Representations (ICLR)*, ser. ICLR’17, Toulon, France, 2017.
- [60] P. W. Battaglia, J. B. Hamrick, V. Bapst, A. Sanchez-Gonzalez, V. Zambaldi, M. Malinowski, A. Tacchetti, D. Raposo, A. Santoro, R. Faulkner, C. Gulcehre, F. Song, A. Ballard, J. Gilmer, G. Dahl, A. Vaswani, K. Allen, C. Nash, V. Langston, C. Dyer, N. Heess, D. Wierstra, P. Kohli, M. Botvinick, O. Vinyals, Y. Li, and R. Pascanu, “Relational Inductive Biases, Deep Learning, and Graph Networks,” 2018, arXiv:1806.01261.
- [61] F. Gama, E. Isufi, G. Leus, and A. Ribeiro, “Graphs, Convolutions, and Neural Networks: From Graph Filters to Graph Neural Networks,” *IEEE Signal Processing Magazine*, vol. 37, no. 6, pp. 128–138, 2020.
- [62] E. Agustsson, F. Mentzer, M. Tschannen, L. Cavigelli, R. Timofte, L. Benini, and L. Van Gool, “Soft-to-Hard Vector Quantization for End-to-End Learning Compressible Representations,” in *Proceedings of the 31st International Conference on Neural Information Processing Systems (NeurIPS)*. Long Beach, California, USA: Curran Associates Inc., 2017, pp. 1141–1151.
- [63] E. Jang, S. Gu, and B. Poole, “Categorical Reparameterization with Gumbel-Softmax,” in *Proceedings of the 5th International Conference on Learning Representations (ICLR)*, Toulon, France, 2017.
- [64] J. R. Magnus, “On Differentiating Eigenvalues and Eigenvectors,” *Econometric Theory*, vol. 1, no. 2, pp. 179–191, 1985.
- [65] S. P. Boyd and L. Vandenberghe, *Convex Optimization*. Cambridge, UK ; New York: Cambridge University Press, 2004.
- [66] H. Amann and J. Escher, *Analysis II*. Basel: Birkhäuser, 2008.
- [67] A. Agrawal, B. Amos, S. Barratt, S. Boyd, S. Diamond, and J. Z. Kolter, “Differentiable Convex Optimization Layers,” in *Proceedings of the 33rd Conference on Advances in Neural Information Processing Systems (NeurIPS)*. Red Hook, NY, USA: Curran Associates Inc., 2019, pp. 9562–9574.
- [68] M. Blondel, Q. Berthet, M. Cuturi, R. Frostig, S. Hoyer, F. Llinares-López, F. Pedregosa, and J.-P. Vert, “Efficient and Modular Implicit Differentiation,” in *Proceedings of the 36th International Conference on Neural Information Processing Systems (NeurIPS)*. Red Hook, NY, USA: Curran Associates Inc., 2022, pp. 5230–5242.
- [69] A. Gershman, N. Sidiropoulos, S. Shahbazpanahi, M. Bengtsson, and B. Ottersten, “Convex Optimization-Based Beamforming,” *IEEE Signal Processing Magazine*, vol. 27, no. 3, pp. 62–75, 2010.
- [70] Y. Huang and D. P. Palomar, “Rank-Constrained Separable Semidefinite Programming With Applications to Optimal Beamforming,” *IEEE Transactions on Signal Processing*, vol. 58, no. 2, pp. 664–678, 2010.
- [71] Y. Nandwani, A. Pathak, Mausam, and P. Singla, “A Primal Dual Formulation for Deep Learning with Constraints,” in *Proceedings of the 33rd International Conference on Neural Information Processing Systems (NeurIPS)*, vol. 32. Red Hook, NY, USA: Curran Associates, Inc., 2019, pp. 12 179–12 190.
- [72] L. Adam and M. Branda, “Machine Learning Approach to Chance-Constrained Problems: An Algorithm Based on the Stochastic Gradient Descent,” 2019, arXiv:1905.10986.
- [73] Q. Hu, Y. Cai, K. Kang, G. Yu, J. Hoydis, and Y. C. Eldar, “Two-Timescale End-to-End Learning for Channel Acquisition and Hybrid Precoding,” *IEEE Journal on Selected Areas in Communications*, vol. 40, no. 1, pp. 163–181, 2022.
- [74] I. Loshchilov and F. Hutter, “Decoupled Weight Decay Regularization,” in *Proceedings of the 7th International Conference on Learning Representations (ICLR)*, 2019, pp. 1–11.
- [75] P. Seetharaman, G. Wichern, B. Pardo, and J. L. Roux, “Autoclip: Adaptive Gradient Clipping for Source Separation Networks,” in *2020 IEEE 30th International Workshop on Machine Learning for Signal Processing (MLSP)*. Espoo, Finland: IEEE, 2020, pp. 1–6.
- [76] L. Schynol and M. Pesavento, “Adaptive Anomaly Detection in Network Flows with Low-Rank Tensor Decompositions and Deep Unrolling,” *IEEE Open Journal of Signal Processing*, vol. 6, pp. 417–433, 2025.
- [77] S. Ioffe and C. Szegedy, “Batch Normalization: Accelerating Deep Network Training by Reducing Internal Covariate Shift,” in *Proceedings of the 32nd International Conference on Machine Learning*, ser. ICML’15, vol. 37. JMLR.org, 2015, pp. 448–456.
- [78] A. Forenza, D. Love, and R. Heath, “Simplified Spatial Correlation Models for Clustered MIMO Channels With Different Array Configurations,” *IEEE Transactions on Vehicular Technology*, vol. 56, no. 4, pp. 1924–1934, 2007.
- [79] R. M. Dreifuerst and R. W. Heath, “Machine Learning Codebook Design for Initial Access and CSI Type-II Feedback in Sub-6-GHz 5G NR,” *IEEE Transactions on Wireless Communications*, vol. 23, no. 6, pp. 6411–6424, 2024.
- [80] 3GPP, “Physical Layer Procedures for Data,” 3rd Generation Partnership Project (3GPP), Tech. Rep. TS 38.214, 2022, version 17.1.0.
- [81] A. Hjørungnes, *Complex-Valued Matrix Derivatives: With Applications in Signal Processing and Communications*, 1st ed. USA: Cambridge University Press, 2011.
- [82] H. Boche and M. Schubert, “A General Duality Theory for Uplink and Downlink Beamforming,” in *Proceedings IEEE 56th Vehicular Technology Conference*. Vancouver, BC, Canada: IEEE, 2002, pp. 87–91.



in 2023.

**Lukas Schynol** (Graduate Student Member, IEEE) received the M.Sc. degree in 2021 in electrical engineering from Technical University of Darmstadt, Darmstadt, Germany, where he is currently working towards the Ph.D. degree. His research interests include resource allocation and anomaly detection in wireless networks using model-aided deep learning. He received the best student paper award (2nd place) at the IEEE International Workshop on Computational Advances in Multi-Sensor Adaptive Processing (CAMSAP)



**Marius Pesavento** (Senior Member, IEEE) received the Dipl.-Ing. and Ph.D. degrees from Ruhr-Universität Bochum, Germany, in 1999 and 2005, respectively, and the M.Eng. degree from McMaster University, Hamilton, ON, Canada, in 2000. From 2005 to 2008, he was a Research Engineer with two start-up companies. He became an Assistant Professor in 2010 and a Full Professor (W3) of Communication Systems in 2013 in the Department of Electrical Engineering and Information Technology, Technische Universität

Darmstadt, Germany. His research interests include statistical and sensor array signal processing, MIMO communications, optimization, and model-assisted deep learning.

He is the Regional Director-at-Large for Region 8 (2025–2027) and a member of the IEEE Signal Processing Society Board of Governors. He is the Editor-in-Chief (2026–2028) of the IEEE Open Journal of Signal Processing (Deputy Editor-in-Chief, 2025; Senior Area Editor, 2019–2024). He was an Associate Editor of the IEEE Transactions on Signal Processing (2012–2016) and a Subject Editor of the EURASIP Journal on Signal Processing (2024–2025; Handling Editor, 2011–2023). He is a member of the “Signal Processing Theory and Methods” Technical Committee (since 2021), served as Vice-Chair of the IEEE SPS “Sensor Array and Multichannel Signal Processing” Technical Committee in 2025 (member, 2012–2017), and is Past Chair of the EURASIP “Signal Processing for Multisensor Systems” Technical Area Committee.